2020

Paleoenvironments, taphonomy, and stable isotopic content of the terrestrial, fossil-vertebrate–bearing sequence of the El Disecado Member, El Gallo Formation, Upper Cretaceous, Baja California, México

David Fastovsky
University of Rhode Island, defastov@uri.edu

Marisol Montellano-Ballesteros

Henry C. Fricke

Jahandar Ramezani

Kaori Tsukui

See next page for additional authors

Citation/Publisher Attribution

Fastovsky, D. E., Montellano-Ballesteros, M., Fricke, H. C., Ramezani, J., Tsukui, K., Wilson, G. P.,...Alvarez, A. (2020). Paleoenvironments, taphonomy, and stable isotopic content of the terrestrial, fossil-vertebrate–bearing sequence of the El Disecado Member, El Gallo Formation, Upper Cretaceous, Baja California, México. *Geosphere, 16*(4), 991-1011. https://doi.org/10.1130/GES02207.1
Available at: https://doi.org/10.1130/GES02207.1

Paleoenvironments, taphonomy, and stable isotopic content of the terrestrial, fossil-vertebrate–bearing sequence of the El Disecado Member, El Gallo Formation, Upper Cretaceous, Baja California, México

Authors

David Fastovsky, Marisol Montellano-Ballesteros, Henry C. Fricke, Jahandar Ramezani, Kaori Tsukui, Gregory P. Wilson, Paul Hall, Rene Hernandez-Rivera, and Geraldo Alvarez

Creative Commons License

This work is licensed under a Creative Commons Attribution-Noncommercial 4.0 License

Research Paper

GEOSPHERE

GEOSPHERE, v. 16, no. 4

https://doi.org/10.1130/GES02207.1

18 figures; 3 tables; 1 supplemental file

CORRESPONDENCE: defastov@uri.edu

CITATION: Fastovsky, D.E., Montellano-Ballesteros, M., Fricke, H.C., Ramezani, J., Tsukui, K., Wilson, G.P., Hall, P., Hernandez-Rivera, R., and Alvarez, G., 2020, Paleoenvironments, taphonomy, and stable isotopic content of the terrestrial, fossil-vertebrate bearing sequence of the El Disecado Member, El Gallo Formation, Upper Cretaceous, Baja California, México: Geosphere, v. 16, no. 4, p. 991–1011, https://doi.org/10.1130/GES02207.1.

Science Editor: Andrea Hampel
Associate Editor: Cathy Busby

Received 22 October 2019
Revision received 30 March 2020
Accepted 19 May 2020

Published online 30 June 2020

Paleoenvironments, taphonomy, and stable isotopic content of the terrestrial, fossil-vertebrate–bearing sequence of the El Disecado Member, El Gallo Formation, Upper Cretaceous, Baja California, México

David E. Fastovsky[1], Marisol Montellano-Ballesteros[2], Henry C. Fricke[3], Jahandar Ramezani[4], Kaori Tsukui[4], Gregory P. Wilson[5], Paul Hall[6], Rene Hernandez-Rivera[2], and Geraldo Alvarez[2]

[1]Department of Geosciences, University of Rhode Island, 9 East Alumni Avenue, Kingston, Rhode Island 02881, USA
[2]Universidad Autónoma Nacional de México, Instituto de Geología, Ciudad Universitaria, Coyahuacán, 04510, D.F. México
[3]Colorado College, Colorado Springs, Colorado 80903, USA
[4]Massachusetts Institute of Technology Earth, Atmospheric and Planetary Sciences, 77 Massachusetts Avenue, Bldg. 54-1116, Cambridge, Massachusetts 02139, USA
[5]University of Washington, Department of Biology, Box 351800, Seattle, Washington 98195-1800, USA
[6]Center for Computation and Visualization, 180 George Street, Brown University, Providence, Rhode Island 02912, USA

ABSTRACT

The Late Campanian (Late Cretaceous), upper part of the El Disecado Member, El Gallo Formation, Baja California, México, preserves a rich fossil assemblage of microvertebrates and macrovertebrates, silicified logs, macroscopic plant remains, and pollen that was likely deposited as the distal part of a subaerial fan. The unit was episodic and high energy, with its salient features deriving from active river channels and sheet, debris-flow deposits. Landscape stability is indicated by the presence of compound paleosol horizons, containing Fe_2O_3 mottling in B horizons, cutans, and calcium carbonate concretions. All of these features indicate wet/dry cyclicity in subsurface horizons, likely attributable to such cyclicity in the climate. Drainage was largely to the north and to a lesser extent, the west; however, some current flow to the south and east is preserved which, in conjunction with the proximal location of marginal marine deposits, suggest the influence of tides in this setting.

The fossil vertebrates preserved in this part of the El Disecado Member are almost exclusively allochthonous, preserved as disarticulated isolated clasts in hydraulic equivalence in the braided fluvial system. A relatively diverse microvertebrate assemblage is preserved, the largest components of which are first, dinosaurs, and second, turtles. Non-tetrapod fossils are relatively uncommon, perhaps reflecting an absence of permanent standing water in this depositional setting.

Here we report a high-precision U-Pb date of 74.706 + 0.028 Ma (2σ internal uncertainty), obtained from zircons in an airfall tuff. The tuff is located low within the sequence studied; therefore, most of the sedimentology and fossils reported here are slightly younger. This date, which improves upon previously published $^{40}Ar/^{39}Ar$ geochronology, ultimately allows for comparison of these El Gallo faunas and environments with coeval ones globally.

Primary stable isotopic nodules associated with roots in the paleosols of the terrestrial portion of the El Disecado Member are compared with ratios from similar sources from coeval northern and eastern localities in North America. Distinctive latitudinal gradients are observed in both $\delta^{13}C$ and $\delta^{18}O$, reflecting the unique southern and western, coastal geographic position of this locality. These differences are best explained by differences in the floras that populated the northern and eastern localities, relative to the southern and western floras reported here.

RESUMEN

La parte superior del Miembro El Disecado de la formación El Gallo, Baja California, México, Campaniano Tardío (Cretácico Tardío), conserva una asociación fósil rica en microvertebrados y macrovertebrados, troncos silicificados, restos macroscópicos de plantas, y polen, la cual fue depositada posiblemente en la parte distal de un abanico subaéreo. La unidad fue depositada de forma episódica y bajo una alta energía, siendo sus rasgos más característicos canales de ríos trenzados y depósitos de flujos de escombros. La estabilidad del paisaje está indicada por la presencia de horizontes compuestos de paleosuelos que contienen horizontes B con un moteado de Fe_2O_3, cutans, y concreciones de carbonato de calcio. Todos estos rasgos indican una ciclicidad de humedad/aridez en horizontes debajo de la superficie atribuibles, probablemente, a la ciclicidad en el clima. El drenaje estaba orientado principalmente hacia el norte y en menor grado al oeste; sin embargo, se conservan algunas corrientes de flujo dirigidas hacia el sur y este, las cuáles junto con la ubicación proximal de los depósitos marinos marginales, sugieren la influencia de mareas en este ambiente.

Los vertebrados fósiles preservados en esta parte del Miembro El Disecado son casi exclusivamente alóctonos, se conservan como clastos aislados desarticulados en equivalente hidraúlico "hydraulic equivalence" en el sistema fluvial trenzado. Una asociación de microvertebrados relativamente diversa se conserva; los componentes más grandes son, en primer lugar, los dinosaurios y en segundo, las tortugas. Fósiles no tetrápodos son relativamente raros, reflejando probablemente

la ausencia de agua permanente en este ambiente de depósito.

Aquí reportamos una edad U-Pb de alta precisión de 74.706 + 0.028 Ma (2σ de incertidumbre interna), obtenida de zircones de una toba de caída "airfall." La toba está localizada en la parte inferior de la secuencia estudiada; por lo tanto, casi toda la sedimentología y fósiles registrados aquí son ligeramente más jóvenes. Esta fecha perfecciona la geocronología $^{40}Ar/^{39}Ar$ publicada previamente, y por último permite la comparación de la fauna y el ambiente de El Gallo con otros contemporáneos.

Proporciones primarias de isótopos estables ($\delta^{13}C$; $\delta^{18}O$) obtenidas de dientes aislados de hadrosaurio (dinosaurio) y de nódulos de carbonato asociados con raíces en los paleosuelos de la parte continental del Miembro El Disecado fueron comparadas con proporciones de fuentes similares de localidades norteñas y orientales contemporáneas en América del Norte. Gradientes latitudinales distintivos fueron observados en $\delta^{13}C$ y $\delta^{18}O$, reflejando la singular posición geográfica costera al sur y occidente de esta localidad. Estas diferencias se explican mejor por las diferencias en las floras que habitaron las localidades norteñas y orientales relativas a las sureñas y occidentales registradas aquí.

INTRODUCTION

The Upper Cretaceous El Disecado Member of the El Gallo Formation (Kilmer, 1963), Baja California, México, has proven to be an abundant source of late Campanian fossil material. Fieldwork from the mid-1960s (Morris, 1973) and regular (yearly) collection, since 2004, of microvertebrates by researchers from the Instituto de Geología Universidad Nacional Autónoma de México (UNAM), the Los Angeles Country Museum, the Universities of Washington and Rhode Island (USA), and some affiliates, have produced a significant assemblage of macro- and micro-terrestrial vertebrates, including dinosaur and mammalian material (e.g., Romo de Vivar Martínez, 2011; López-Conde et al., 2018). A floral assemblage, dominated by fossil fruits, is also preserved (Hayes et al., 2018), along with an extensive undescribed palynoflora.

These Late Cretaceous fossil localities from the west coast of North America contain the southernmost and westernmost fossil vertebrates known from the Campanian of North America, and thus provide a biogeographically unique datum for comparison with better known, contemporaneous North American Campanian terrestrial biotas to the north and east. Here, we situate this fossil assemblage in its paleoenvironmental, taphonomic, and stratigraphic contexts. We present evidence that this portion of the El Disecado Member, here termed the Fossiliferous Terrestrial Sedimentary Sequence (FTS), represents a physically active and biologically productive distal terrestrial fan deposit, built by a sandy low-sinuosity fluvial system forming in a cyclical wet/dry climatic setting. Our new high-precision U-Pb zircon age from this member improves upon its legacy $^{40}Ar/^{39}Ar$ geochronology and helps place its rich fossil fauna in its regional biostratigraphic context.

To enrich our understanding of the context of the vertebrates, we analyzed stable isotopic ratios (^{18}O and ^{13}C) retrieved from both the teeth of hadrosaurs (dinosaurs) and from paleosol carbonates. These ratios allowed for comparison with approximately coeval isotopic data from much better known Campanian localities in the United States and Canada, and the isotopic ratios recovered from the El Disecado Member fit well into latitudinal isotopic trends observed in those regions.

Setting, Geological Context, and Stratigraphic Relationships of the El Disecado Member of the El Gallo Formation

The El Gallo Formation outcrops in the modern Peninsular Ranges, a low suite of mountains that lines the western part of Baja California. These mountains formed in a forearc basin, the result of arc magmatism driven by Late Cretaceous–early Paleocene subduction in northwestern Baja California (Busby et al., 1998, 2002; Busby, 2004). Busby et al. (1998) described strike-slip basin formation, tilting, and associated uplift to produce a thick sequence of outcrops including those described here.

Kilmer (1963) first described the El Gallo Formation as a ~1300-m-thick sequence of terrestrial sedimentary rocks composed of three members (in ascending order): La Escarpa, El Disecado, and El Castillo, the last of which is encompassed within the El Disecado Member and restricted to the eastern side of the basin (Figs. 1 and 2).

Fulford and Busby (1993, p. 302) characterized the El Gallo Formation as a "retrogradational sequence of alluvial plain through floodplain deposits capped by tidal deposits" within a forearc basin. They recognized four "successions," of which Successions 2–4 constitute the El Disecado Member of Kilmer (1963). The FTS is correlative with the uppermost part of Succession 2 and most of Succession 3. It constitutes ~130 m, running from local sea level upsection to the stratigraphic level in which the El Disecado Member begins to produce marine fossils. Previous $^{40}Ar/^{39}Ar$ geochronology (Renne et al., 1991) determined a Campanian (Late Cretaceous) age for the El Gallo Formation and its vertebrate fauna (Fig. 2).

METHODS

U-Pb Geochronology

Tuff layers preserved in the FTS were sampled for U-Pb geochronology by chemical abrasion–isotope dilution–thermal ionization mass spectrometry (CA-ID-TIMS), following the general procedures described in Ramezani et al. (2011). The sample was disaggregated by standard crushing methods and heavy-mineral concentrates were obtained using a Frantz® magnetic separator and high-density liquids. Zircons were hand selected under a binocular microscope and pretreated by a chemical abrasion technique modified after Mattinson (2005); this technique involved thermal annealing in a furnace at 900 °C for 60 h, followed by partial dissolution in 29M HF at 210 °C in high-pressure vessels for 12 h. The chemically abraded grains were fluxed in and rinsed with several hundred microliters of dilute HNO_3, 6M HCl and Millipore water, successively on the hot plate and in an ultrasonic bath, to remove the leachates.

Thoroughly rinsed zircon grains were spiked with the EARTHTIME ET535 mixed ^{205}Pb-^{233}U-^{235}U

isotopic tracer (Condon et al., 2015; McLean et al., 2015) prior to complete dissolution in 29M HF at 210 °C for 48 h and subsequent Pb and U purification via an HCl-based anion-exchange column chemistry (Krogh, 1973). Pb and U were loaded together onto single outgassed Re filaments along with a silica-gel emitter solution, and their isotopic ratios were measured on an Isotopx X62 multi-collector thermal ionization mass spectrometer equipped with a Daly photomultiplier ion-counting system at Massachusetts Institute of Technology. Pb isotopes were measured as mono-atomic ions in a peak-hopping mode on the ion counter, whereas U isotopes were measured as dioxide ions in a static mode using three Faraday collectors. A predicted sample $^{238}U/^{235}U$ ratio of 137.818 ± 0.045 (Hiess et al., 2012) was used in age calculation, along with an oxide correction based on an independently determined $^{18}O/^{16}O$ ratio of 0.00205 ± 0.00005.

Data reduction, calculation of dates, and propagation of uncertainties used the Tripoli and ET_Redux applications and algorithms (Bowring et al., 2011; McLean et al., 2011). The individual $^{206}Pb/^{238}U$ dates were corrected for initial ^{230}Th disequilibrium based on a magma Th/U ratio of 2.8 ± 1.0 (2σ). The sample age was calculated based on the weighted-mean $^{206}Pb/^{238}U$ date of all of the analyses without any exclusions and reported with 95% confidence level uncertainties including both internal (analytical) uncertainty and total propagated uncertainty (in brackets), which included the decay constant uncertainties of Jaffey et al. (1971). The total uncertainty must be taken into account when dates from different chronometers (e.g., U-Pb of this study versus $^{40}Ar/^{39}Ar$ of Renne et al., 1991) are compared.

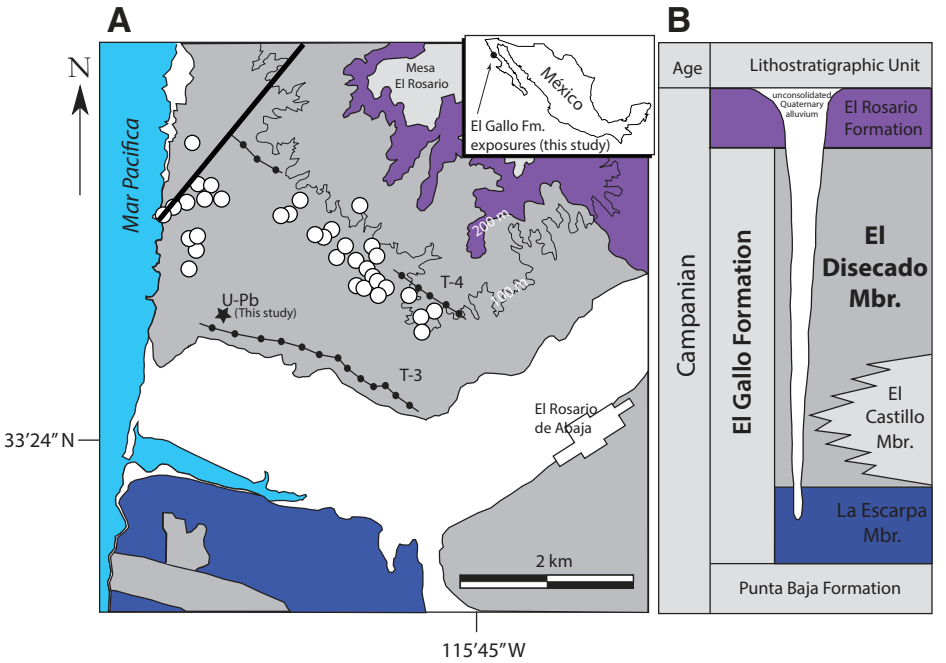

Figure 1. (A) Simplified geologic map of the fossiliferous terrestrial sequence (FTS) part of the El Disecado Member, El Gallo Formation. Inset: El Rosario, Baja California, México. (B) Lithostratigraphic relationships of Campanian units, modified after Fulford and Busby (1993). Open circles represent locations of 738 fossiliferous localities of this study. Tuff layer samples of Fulford and Busby (1993), labeled T-3 and T-4, previously dated by the ^{40}Ar-^{39}Ar method (Renne et al., 1991) are indicated. Star indicates location of ^{238}U-^{206}Pb geochronology sample of this study; line represents location of FTS generalized section shown in Figure 2.

Sedimentary Geology

Paleoenvironments of the FTS were reconstructed via a conventional sedimentological approach (Graham, 1988), using a combination of 21 stratigraphic sections measured with a Jacob's staff at key vertebrate-producing localities, observation of sandbody geometries, lithologies and sedimentary structures preserved in outcrop, measurement of cross-stratification orientations, and hand samples collected for laboratory analysis. From these data, we reconstructed minimum bedform sizes, from which we then deduced the intensities and directions of ancient flows.

GPS coordinates were recorded for all localities. These coordinates were mapped in Google Earth Pro (v. 7.3.2.5776–64 bit) and were then transferred to a 1:50,000 topographic map, "El Rosario de Arriba," published by the Mexican governmental cartographic authority INEGI (www.inegi.gob.mx; 2003). This map served as the base map for all of the work reported here.

For grain-size determination, samples were soaked overnight in a 5% Calgon deionized water solution to deflocculate clays, and then were analyzed on a Malvern "Mastersizer 3000" laser-diffraction grain-size analyzer. Petrographic analysis was carried out using 30μ thin sections studied under an Olympus BH-2 petrographic microscope with an Olympus DP-73 camera attached.

Apparent paleocurrent flow directions were measured with a leveled Brunton compass, oriented to obtain the direction of the maximum dips of cross stratification as exposed in three dimensions. Ancient flow directions were ultimately reconstructed by (1) correction of initial trend readings for declination (10.5° east); (2) removal of structural dip (e.g., the trend measurements were rotated to flatness using Stereonet v. 9.9.6 for Mac), and (3) 8.6° counterclockwise rotation of modified dip orientations, undoing the clockwise

rotation they underwent in the past 12 m.y. associated with the active period of the opening of the Gulf of California (DeMets and Merkouriev, 2016). Rose diagrams and statistics were generated using MatLab; statistical calculations are after Graham (1988).

Vertebrate Fossil Collection

Microvertebrates, the focus of the paleontological work reported here, were obtained by close surface prospecting and, when bone (generally, tiny fragments) was found, collecting sedimentary rock at the site in large bags for screen washing. Each of these collections of rock constitutes a locality (see "Vertebrate assemblages" below), and we returned annually to the most productive of them for more rock matrix (and microfossil) collection.

By far the greatest preponderance of microfossil retrieval was obtained by screen washing. Screen washing was performed by soaking the rock matrix overnight in water, followed by screening. The concentrate was then handpicked under a magnifying lens. On average, a single vertebrate microfossil is produced from every 23 kg of bulk-collected FTS matrix.

Stable Isotopes

Hadrosaur teeth were collected from a single FTS microfossil locality, ROS-50. Paleosol carbonate nodules were collected from two localities, "Silvinia" and "Granito de Mostaza" (all locality data available at the Instituto de Geología, UNAM). Tooth enamel, tooth dentine, and pedogenic carbonate samples weighing ~1 mg were extracted using a diamond-tipped Dremel drill. Samples were then soaked in 0.1 M acetic acid for 24 h, rinsed three times with deionized water and then dried for 24 h. This removed any secondary authigenic carbonate.

Carbon- and oxygen-isotope ratios were obtained using an automated carbonate preparation device (KIEL-III) and a Finnegan MAT 252 isotope ratio mass spectrometer at the University of Arizona in Tucson. The isotope ratio measurement is calibrated based on repeated measurements of National Bureau of Standards (NBS)-19 ($\delta^{18}O$ = –2.20‰, $\delta^{13}C$ = +1.95‰), NBS-18 ($\delta^{18}O$ = –23.20‰, $\delta^{13}C$ = – 5.01‰), and CAR-1, an in-house carbonate standard ($\delta^{18}O$ = –1.41‰, $\delta^{13}C$ = +2.03‰). Analytical precision is ±0.1‰ for both carbon and oxygen. Isotope ratios are reported using the "δ" notation with $\delta^{13}C$ and $\delta^{18}O$ referring to $(R_{sample}/R_{standard} - 1) \times 1000‰$, where R is the ratio of the heavy isotope to the light isotope for carbon and oxygen, respectively. The standard for carbon is Vienna Pee Dee Belemnite (VPDB), and the standard for oxygen is Vienna Standard Mean Ocean Water (VSMOW).

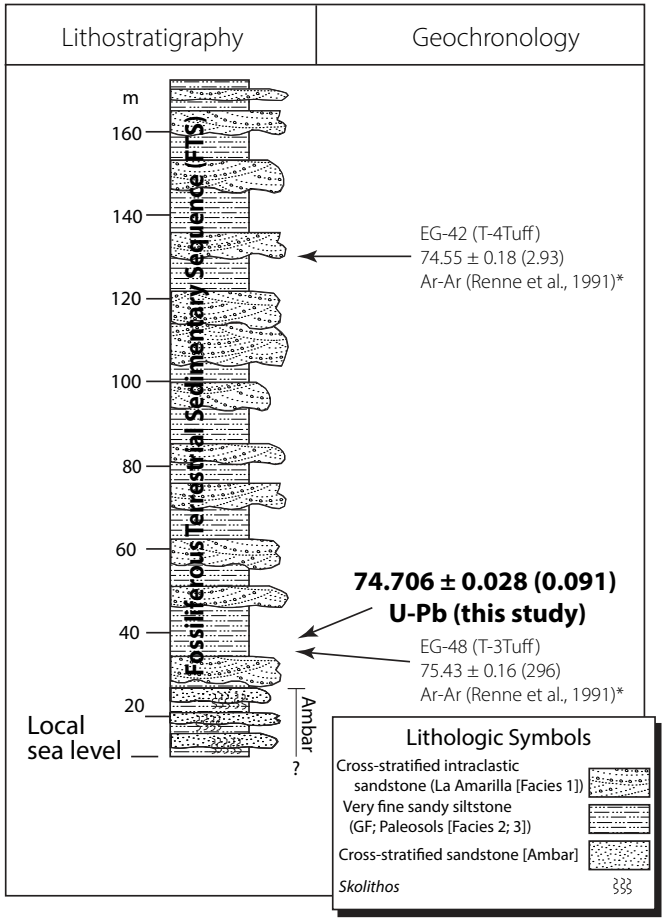

Figure 2. Lithostratigraphy and geochronology of the upper El Discado Member of the El Gallo Formation comprising the fossiliferous terrestrial sequence (FTS). See Figure 1A for section location. Projected levels corresponding to legacy Ar-Ar geochronology samples EG-42 and EG-48 of Renne et al. (1991) or T-4 and T-3 tuff layers of Fulford and Busby (1993) are indicated. *Recalculated using revised Ar-Ar age calculation parameters (see text for details).

RESULTS AND INTERPRETATIONS

Depositional Age

A suite of four closely spaced (~50 cm) indurated ash tuffs, recognizable by phenoclasts of plagioclase, quartz, biotite, and other minerals in a clay-rich matrix, was present in an outcrop near

TABLE 1. U-Pb ISOTOPE DATA FOR THE ANALYZED ZIRCONS FOR THE EL GALLO FORMATION TUFF (SEE FIG. 3)

Sample fractions (a)	Pb(c) (pg) (b)	Pb* / Pb(c)	U (pg) (c)	Th / U	Ratios								Ages (Ma)						
					$^{206}Pb/^{204}Pb$ (d)	$^{208}Pb/^{206}Pb$ (e)	$^{206}Pb/^{238}U$ (f)	Error (2σ%)	$^{207}Pb/^{235}U$ (f)	Error (2σ%)	$^{207}Pb/^{206}Pb$ (f)	Error (2σ%)	$^{206}Pb/^{238}U$	Error (2σ)	$^{207}Pb/^{235}U$	Error (2σ)	$^{207}Pb/^{206}Pb$	Error (2σ)	Corr. coef.
Ceniza																			
z4	0.44	57.8	2010	0.69	3290.1	0.221	0.011662	(0.07)	0.07704	(0.42)	0.04794	(0.39)	**74.742**	**0.050**	75.36	0.30	95.0	9.3	0.43
z3	0.39	24.3	786	0.50	1466.8	0.160	0.011657	(0.09)	0.07718	(0.89)	0.04804	(0.86)	**74.711**	**0.066**	75.49	0.65	100	20	0.33
z2	0.66	25.0	1349	0.57	1482.0	0.182	0.011656	(0.09)	0.07697	(0.88)	0.04792	(0.86)	**74.702**	**0.064**	75.29	0.64	94	20	0.29
z1	0.42	46.1	1394	1.04	2417.1	0.332	0.011651	(0.07)	0.07679	(0.53)	0.04783	(0.51)	**74.670**	**0.049**	75.13	0.39	90	12	0.33

(a) Thermally annealed and pre-treated single zircon. Data used in age calculation are in bold.
(b) Total common-Pb in analyses.
(c) Total sample U content.
(d) Measured ratio corrected for spike and fractionation only.
(e) Radiogenic Pb ratio.
(f) Corrected for fractionation, spike, and blank. Also corrected for initial Th/U disequilibrium using radiogenic ^{208}Pb and Th/U_{magma} = 2.8.
Notes: Mass fractionation correction of 0.18%/amu ± 0.04%/amu (atomic mass unit) was applied to single-collector Daly analyses. All common Pb assumed to be laboratory blank. Total procedural blank less than 0.1 pg for U. Blank isotopic composition: $^{206}Pb/^{204}Pb$ = 18.15 ± 0.47, $^{207}Pb/^{204}Pb$ =15.30 ± 0.30, $^{208}Pb/^{204}Pb$ = 37.11 ± 0.87. Corr. coef. = correlation coefficient. Ages calculated using the decay constants λ_{238} = 1.55125E-10 y^{-1} and λ_{235} = 9.8485E-10 y^{-1} (Jaffey et al., 1971).

the base of the FTS (Fig. 2). Each layer was 3–10 cm thick and preserved within gray siltstones with few distinguishing characteristics (Facies 3). The surficial ash layers we sampled for this study presented, when weathered at the surface, a dried white (7.5PB 9/2; Munsell Soil Color Charts, 1992) appearance with fine sand-sized mafic (biotite?) specks, and when freshly exhumed, a moist greenish gray (5G 5/1 gley; Munsell Soil Color Charts, 1992) aspect. An absence of sedimentary structures and the abundance of clays suggest that these layers represent (primary) airfall tuffs, likely to have been originally composed of a glass-rich matrix.

Complete Pb and U isotopic data are given in Table 1, and the age results are illustrated on the age plots of Figure 3. The stratigraphically highest layer of the tuff suite was sampled for U-Pb zircon geochronology by the cathodoluminescence–isotope dilution–thermal ionization mass spectrometry (CA-ID-TIMS) method (see Methods). Four single zircons analyzed from this sample all overlap in age within uncertainty and yield a weighted-mean $^{206}Pb/^{238}U$ date of 74.706 ± 0.028 (0.091) Ma with a mean square of weighted deviates (MSWD) of 1.4 (Fig. 3). The latter date represents the best estimate for the Campanian deposition of the corresponding strata.

Renne et al. (1991) reported $^{40}Ar/^{39}Ar$ geochronology based on laser-fusion analyses of single sanidine grains from four widely spaced tuff horizons throughout the El Gallo Formation, producing dates that ranged from 74.87 Ma to 73.59 Ma with 2σ analytical uncertainties of ± 0.10 to ± 0.18 m.y. Although this level of age precision (~0.2%) was groundbreaking for its time, later improvements

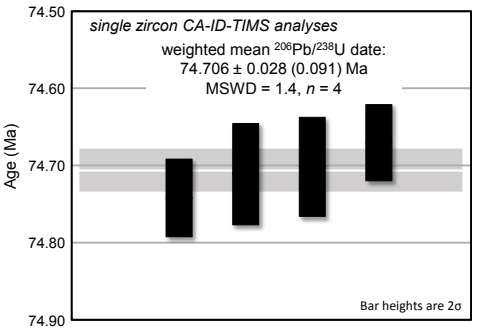

Figure 3. Date distribution plot of zircon cathodoluminescence–isotope dilution–thermal ionization mass spectrometry (CA-ID-TIMS) U-Pb analyzes from the El Gallo Formation tuff. Solid bars are individual zircon analyses. Horizontal shaded band represents the weighted-mean $^{206}Pb/^{238}U$ date and its 95% confidence level internal uncertainty. See Table 1 for complete U-Pb data. MSWD—mean square of weighted deviates.

to the K decay constants (e.g., Min et al., 2000) and the age of the Fish Canyon sanidine fluence monitor (e.g., Kuiper et al., 2008) necessitate revisions to the above dates that exceed the reported uncertainties. Samples EG-48 and EG-42 with recalculated $^{40}Ar/^{39}Ar$ ages (2σ) of 75.17 ± 0.30 (2.96) Ma and 74.55 ± 0.18 (2.93) Ma, respectively, fall within the FTS part of the El Disecado Member (Figs. 1 and 2). Based on previously published map illustrations, we infer that our U-Pb tuff sample and sample EG-48 of Renne et al. (1991 = T3 tuff of Fulford and Busby, 1993) belong to the same stratigraphic level, notwithstanding a lack of precise sample location (e.g., GPS coordinates) for these legacy ages. Considering the large total propagated uncertainties of the $^{40}Ar/^{39}Ar$ dates due to large errors associated with the K decay constants, all three dates tend to overlap within total uncertainty.

Sedimentary Geology

Outcrops associated with the FTS are repetitively yellow- and gray-banded, corresponding to distinct facies (Fig. 4). These are all tilted uniformly throughout the full exposure of the FTS, with strikes of ~120° and dips of ~14° NE, presumably reflecting

Figure 4. Typical exposures of the fossiliferous terrestrial sequence (FTS), El Disecado Member, El Gallo Formation, Baja California, México. Note repetitive yellow and red and gray banded sequences; the yellow is La Amarilla (Facies 1), and the red and gray sequence is Facies 3 (paleosol facies).

the active tectonic history of this unit. Directly adjacent to the Pacific Ocean, there also occur flat-lying, plane-bedded deposits superimposed upon the tilted deposits; we interpret the former to represent Quaternary or Holocene deposition, and thus these deposits do not form a part of this study.

The thicknesses of units within the FTS vary but form a semi-regular interbedded pattern. The contacts between the different colored beds are sharp. In these exposures, we recognize three important facies: (1) a medium- to coarse-grained, iron-stained (yellow), cross-stratified sandstone ("La Amarilla"), which unsurprisingly corresponds to yellow bands in outcrop; (2) a very fine- to fine-grained, gray mud-rich siltstone with variably sized intraclasts (the "GF facies"); and (3) a silt- to very fine-grained gray sandstone with weakly to moderately well-developed pedogenic features including carbonate nodules (the "paleosol facies"). Figure 5 shows some columnar sections measured at several localities; these sections exemplify sedimentary deposition in the FTS.

Facies 1 (La Amarilla)

Description. La Amarilla is an iron-stained, yellow, texturally immature sandstone facies whose medium sand-sized (~0.20–0.28 mm) framework constituents, though moderately well sorted (Fig. 6), are angular (Fig. 7). Compositionally this facies also is immature, including angular clasts of mono- and crypto-crystalline (chert) quartz, plagioclase, K-feldspar, biotite mica, a variety of clay-rich lithic fragments comprising the framework constituents. These are generally concentrated in laminae best measured on decimeter scales or occur as thin linings of concave-upward scour surfaces. The rock is weakly, but pervasively, cemented by clay and calcite cements. Petrographically, the rock suggests a mixed sedimentary and igneous provenance (Fig. 7). The textural and compositional immaturity, the presence of fresh feldspars and micas, in concert with the presence of sedimentary lithic fragments indicate a probable volcanic source with a strong sedimentary influence (such as perhaps a volcanic origin and transport through an eroding southern, sedimentary source). In the scheme of Dickinson and Suczek (1979), this lithology would be classified as having a "magmatic arc" provenance.

Facies 1 exhibits variable thicknesses on a multi-meter scale, ranging from ~1 m to as much as 10 m; however, many of these deposits are multi-storeyed. Individual storeys can be identified by the superposition of channeliform sandstone bodies (Fig. 8A) within the beds (Bridge and Tye, 2000). Although these channels can be stacked and upper channels erode into lower ones (e.g., they are "amalgamated-truncated," sensu Hajek and Heller, 2012), we estimate that individual storeys range from ~1–2 m. Contacts with subjacent units are abrupt and are marked by convex-down (channeliform) shapes (Fig. 9).

The arcuate bases of the cross strata are commonly lined with coarser materials, including chert pebbles, mudstone intraclasts (some as large as 25 cm along the longest axis), petrified tree trunks (up to 6 m), and disarticulated dinosaur (hadrosaur) long bones. All of these features are associated (and commonly aligned) with the features of the sedimentary structures, indicating that they were being carried as intraclasts in the current (Fig. 8B). The width of the channeliform bodies varies; however, in general, these extend 20–40 m.

Internally, La Amarilla is characterized by small-, medium- and large-scale, trough cross stratification throughout (Fig. 8C). In general, the largest scale features in each bed are located basally, and the proportion of smaller-scale cross-stratification increases higher in each storey. We measured the trends of the cross-stratification dip directions to

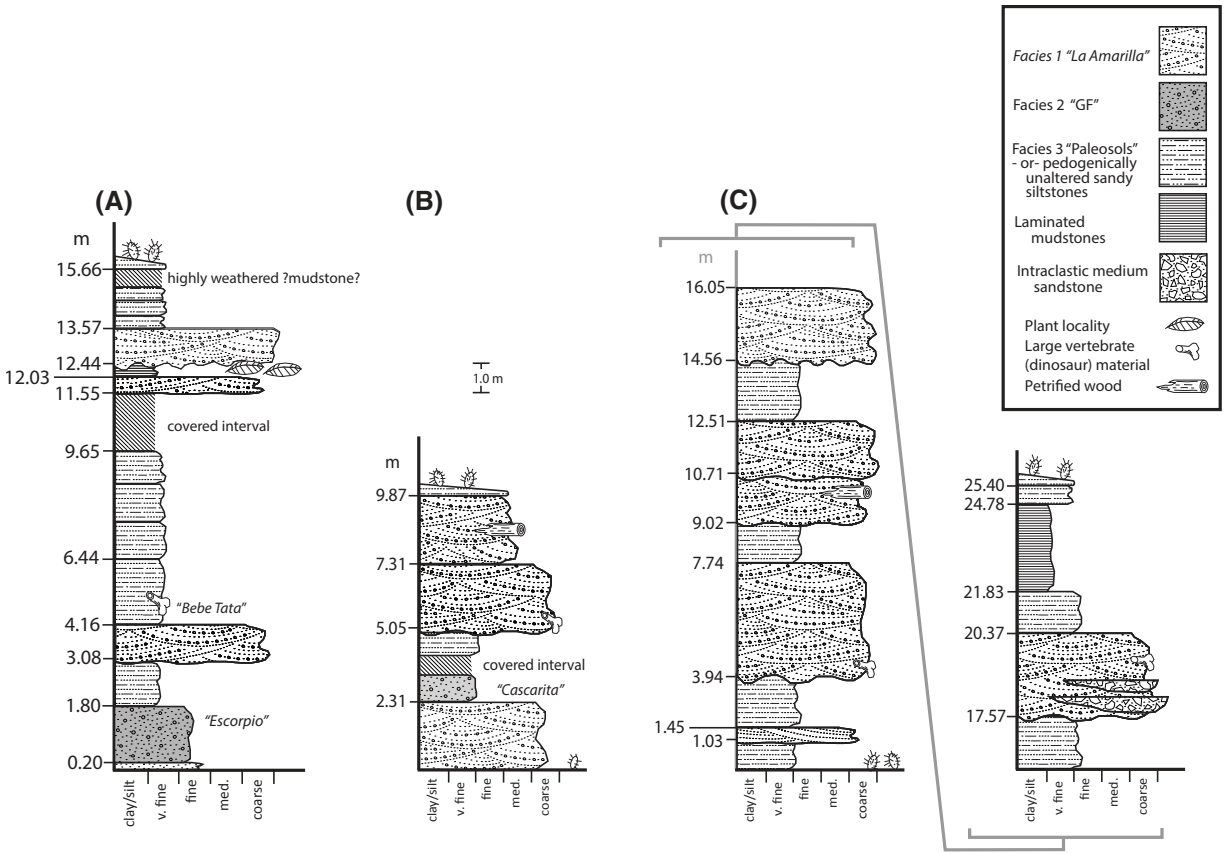

Figure 5. Three measured sections exemplifying fossiliferous terrestrial sequence (FTS) sedimentation, El Gallo Formation, Baja California, México. "Cascarita" and "Escorpio" are microvertebrate-bearing localities. "Bebe Tata" is a baby hadrosaur locality (see text). Locality data are available at the Instituto de Geología, Universidad Autónoma Nacional de México.

reconstruct the ancient paleoflow direction. There is significant variation, but overall they show a dominantly NNW flow (Fig. 10; see below).

Interpretation. We interpret the cross stratification to represent a variety of large-scale sandy bars and smaller, sandy, subaqueous dunes, all migrating under strong unidirectional flows (Leclair and Bridge, 2001; Bridge, 2003). Based upon a rough estimate of the average size of the dune trough cross stratification (~12 cm), dune heights may be inferred to range between 30 and 60 cm, using the method of Leclair and Bridge (2001). From these calculations, water depths of ~3–5 m can be inferred (Bridge and Tye, 2000). These rough relationships allow us to calculate flow intensities in the 100–200 cm/sec range, obtained from grain size and the inferred sizes of bedforms and flow depths (Harms et al., 1982; see also Rubin and McCulloch, 1980 and Bhattacharya et al., 2016). Finally, using the formulation of Lynds et al. (2014), we obtained a slope of 0.00008 for the FTS, an extremely gentle slope of 0.8 m/km. This calculation, like the others, is a rough approximation; however, it gives a general sense of prevailing sedimentary conditions when the FTS part of the El Disecado Member was active.

The shapes of the sedimentary bodies indicate aqueous transport in erosive channels; large mudstone intraclasts and sharp contacts cutting subjacent units reveal the erosion. These channels would have avulsed and/or migrated episodically within a broad floodplain swath, each depositional event beginning with the highest flow intensities, and waning, as reflected by the decrease in the size of the grain sizes and cross stratification upwards in each bed. Distinct channeliform bodies within

this facies (Fig. 8A) suggest that channel migration occurred as much by avulsion as by lateral erosion (see Collinson, 1996; Mohrig et al., 2000).

Sandy bars evidently developed, as indicated by bar-scale cross-stratification (Fig. 8C). However, stabilized (vegetated) bar sedimentary features reported in many braided systems are not preserved (Boothroyd and Ashley, 1975; Miall, 1977, 1978, 2006). This is not unexpected; full channel bodies (surrounded by mudstones) are rarely preserved; instead, most channels and bars have been partially eroded by younger channels and, following the characterization of Hajek and Heller (2012), would be classified as amalgamated to truncated. Taken in total, the evidence indicates that this was an active, episodic, sandy, low-sinuosity channelized fluvial system (Bridge and Tye, 2000; Bridge, 2003).

Facies 2 (GF)

Description. Facies GF is neither volumetrically nor visually distinctive in the FTS; however, it produces microvertebrates (fossils generally but not exclusively <~3 mm on the long axis) and is the most fossiliferous facies in the entire unit; for this reason, and because it bears upon the depositional setting, it commands our attention (Fig. 11A). Facies 2 is near black when moist (N4/ "dark gray"; Munsell Soil Color Charts, 1992); a clay-cemented, silt-to very fine sandstone (Fig. 6). Units are generally 1–2 m in thickness and locally lenticular. Its framework constituents are dominated by silt-sized angular clasts; however, chaotically distributed among these are subrounded to subangular lithic intraclasts ranging from very coarse sand- to granule-sized. These occupy <1% of the sample. The silt- and very fine sand-sized framework fraction of this siltstone consists of quartz, plagioclase, K-feldspar, biotite, and minor muscovite (Fig. 11B). Sedimentary structures are generally not visible in this facies; moreover, the large chert intraclasts are chaotically distributed in the siltstone matrix, in striking contrast to the well-sorted, well-developed, large-scale sedimentary structures visible in Facies 1.

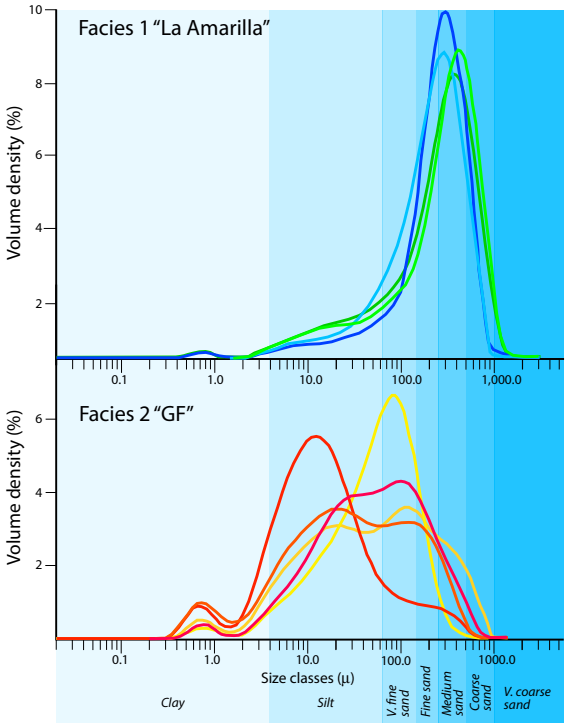

Figure 6. Grain-size distributions for samples of La Amarilla and GF facies. (A) La Amarilla (Facies 1); (B) GF (Facies 2).

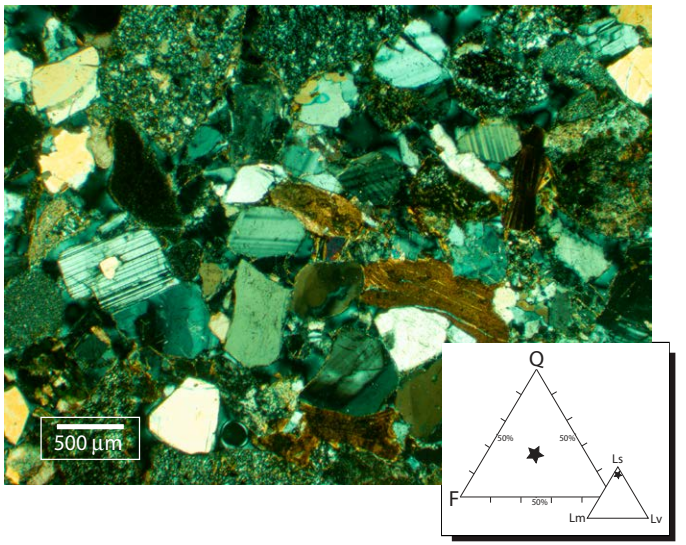

Figure 7. Photomicrograph with crossed polars of Facies 1 (La Amarilla), El Disecado Member, El Gallo Formation, Baja California del Sur, México. Insert: Ternary diagrams showing percentages of quartz (Q), feldspars (F), and lithic fragments, including sedimentary lithic fragments (Ls), volcanic lithic fragments (Lv), and metamorphic lithic fragments (Lm). La Amarilla is moderately well sorted but texturally and compositionally immature (Q33%; F32%; L30%), with a strong sedimentary lithic component (Ls89%; Lv2%; Lm1%).

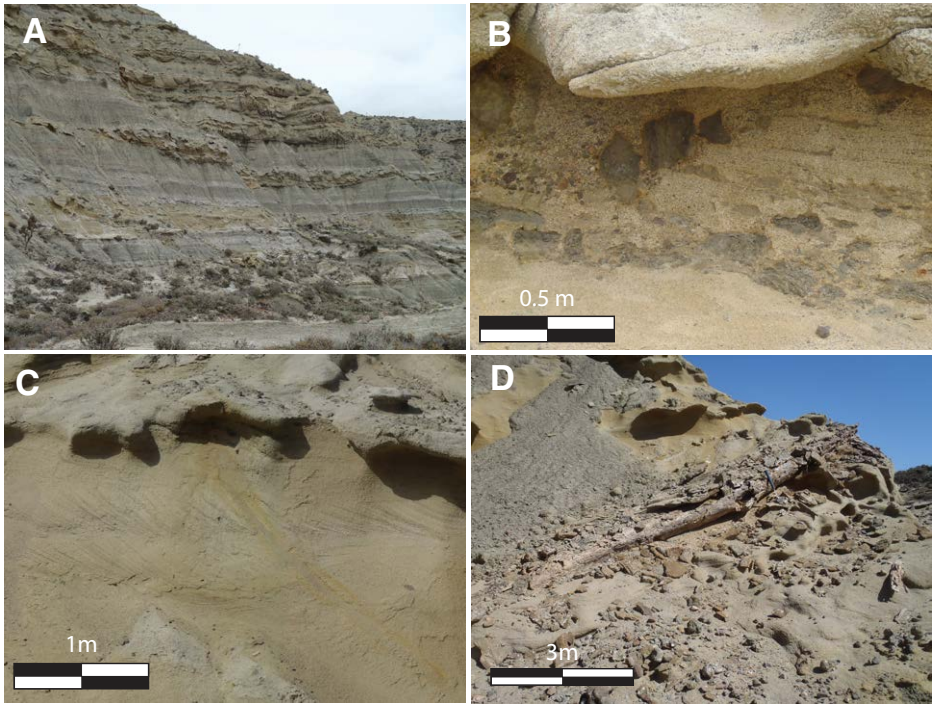

Figure 8. Facies 1—La Amarilla. (A) Unusual channelized exposure (most are amalgamated to truncated, sensu Hajek and Heller, 2012), showing concave-upwards erosive bases and lateral thinning; a local fault accounts for the visible offset in the beds (see Fig. 9 for bedding diagram showing depositional features); (B) mud intraclasts aligned along basal trough scour surfaces; (C) mesoscale cross-trough stratification; (D) petrified log along basal scour surface of a set.

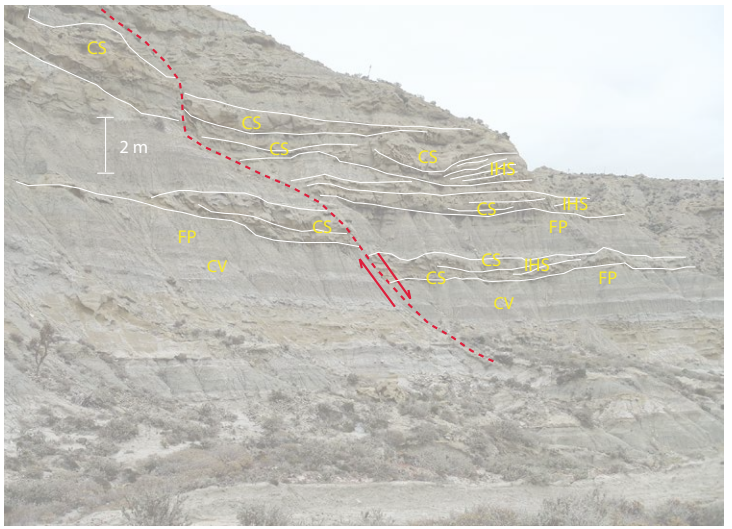

Figure 9. Bedding diagram for Figure 8A, showing key sedimentary depositional features. CS—channel scour; IHS—inclined heterolithic strata (sensu Thomas et al., 1987); FP—floodplain deposits (with paleosols); CV—crevasse splay deposits. Normal fault marked in red dashed line (see text).

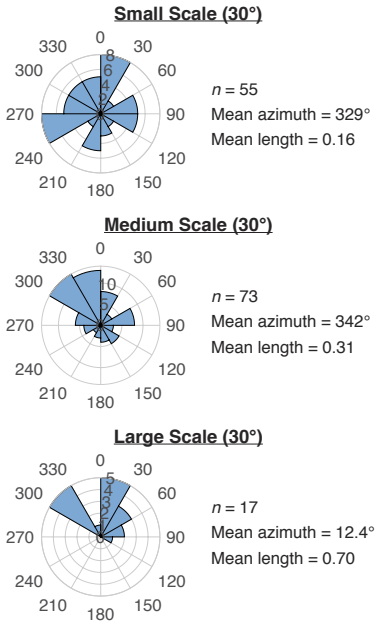

Figure 10. Dip orientations of cross stratification in La Amarilla (Facies 1). Original data presented in the Supplement Material (text footnote 1).

Clays constitute some 20%–30% of this facies (Fig. 6). X-ray diffraction analysis in the laboratory of Dra. T. Pi (Instituto de Geología, UNAM) suggests that the dominant clay species in Facies GF is illite (see Supplemental Material[1]). These clays can appear aligned around the framework clasts, suggesting diagenetic (including pedogenic) alteration and/or recrystallization; ultimately, the contributions of diagenetic and syndepositional clays are impossible to tease apart. However, it is likely that a considerable portion of the clay-sized matrix, only part of which is actually composed of clay minerals, was deposited syndepositionally.

The fossils in Facies 2 (GF) are generally in the 1–3 mm range (although identifiable ones average ~15 mm), and are commonly (but not exclusively) found nearly or completely disarticulated. Microvertebrate remains dominate the collections (Romo de Vivar Martínez, 2011; García-Alcántara, 2016; see below); however, tiny (~3 mm, aperture notch to apex) gastropod shells are also present.

Interpretation. The absence of sedimentary structures or other evidence of internal organization in Facies GF suggests non-Newtonian processes in the form of sediment gravity flows (e.g., Lowe, 1979; Miall, 2006), an interpretation concordant with the high percentages of silt- and clay-sized material in this facies (Fig. 6). The most likely type of flow, suggested by the grain sizes involved, would be hyperconcentrated sheet flows (Pierson and Costa, 1987), in which flow intensities reaching 10 m/sec have been recorded. Sheet flows are concordant with the relatively thin outcrops of this facies. High flow intensities are suggested by the disarticulated, broadly distributed microfossil content of Facies GF. This facies therefore represents a non-channelized, dense, clay- and silt-rich sediment slurry deposited in dramatic density contrast with the air, as a shallow sediment gravity flow at relatively high flow velocities (sensu Fraser and Suttner, 1986; Miall, 2006). Facies 2 (GF) may correspond to Fulford and Busby's (1993) "laminated sand sheet floods," although we did not observe laminations in this facies.

Facies 3 (Paleosols)

Description. Facies 3, which occupies the preponderant portion of the FTS, is composed of a fine-grained suite of deposits showing pedogenic color banding (Figs. 4 and 12A). These units are dominated by clay- and silt-sized fractions. The remainder of the sedimentary rock consists of very fine sand-sized material, including quartz, plagioclase, K-feldspar, and sedimentary lithic fragments. These grains have the same maturity—both textual and compositional—as those in Facies 2.

Horizonation within this facies is commonly distinguished by color or textural changes—and ranges from 0.5–3 m; however, color banding within the bedding, weakly visible on the exterior weathered surface of the outcrop, generally occurs on a smaller scale, ranging from 0.5–1.5 m. The colors include drab grays, reds, and yellows (N5/; 4GY 4/1; 5GY 5/1; 10R 4/6; 2.5Y 6/6; Munsell Soil Color Charts, 1992). The color bands are produced by distinctive ferric oxyhydroxide mottling, best seen in fresh rock samples (Fig. 12B).

Also visible in some—but not all—outcrops are distinctive aggregated blocks of material best interpreted as soil structure (peds). Ped types present include blocky, subangular blocky, and some weakly planar features, likely platy peds (Retallack, 2001). In thin section, the peds reveal themselves to be aggregates of material with well-developed

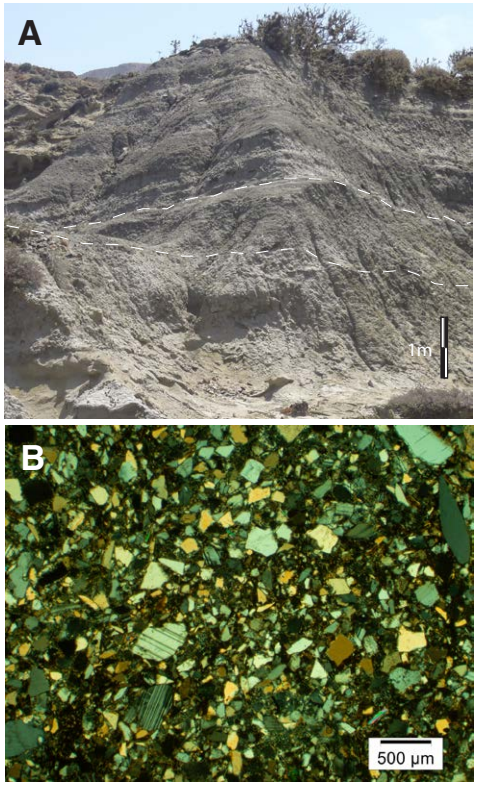

Figure 11. Facies 2, GF. (A) Outcrop view (dashed lines); by comparison to surrounding units Facies GF is not distinguished; however, fresh, slightly dampened samples, reveal a more dark-toned (10Y 2.5/1 "black") color than seen in surrounding units; (B) photomicrograph with crossed polars of Facies GF showing textural and compositional immaturity of the very fine sand-sized (and larger) component of this facies. El Disecado Member, El Gallo Formation, Baja California, México.

Supplement to Fastovsky et al., Paleoenvironments and Taphonomy of the El Disecado Mbr., Upper Cretaceous, Baja California, México

This document contains some of the raw data supporting the work presented in Fastovsky et al., Paleoenvironments and Taphonomy of the El Disecado Mbr., Upper Cretaceous, Baja California, México.

Age

Sedimentology

Petrographic (point count) data from La Amarilla. Cements were largely clays and a smaller percentage of carbonates; we only report framework grains here.

Clast type	Counts	Percentage	Counts	Percentage	Counts	Percentage
Chert	16	6	14	5	14	5
Quartz	69	27	96	34	96	32
Plagioclase	36	14	36	13	43	14
K-feldspar	46	18	60	21	61	20
Lithic (sedimentary)	68	27	70	24	54	18
Lithic (metamorphic)	3	1	0	0	3	1
Lithic (volcanic)	5	2	2	< 1	6	2
Micas (biotite & muscovite)	8	3	8	3	21	7
Carbonates	5	2		< 1	< 1	< 1
Totals	256		286		298	

Dune height (α|) was estimated using the equation of Leclair and Bridge (2001): $\beta=s_{st}/1.5 = 12/1.5$; if $\alpha = 4 - 7$, and s_{st} = thickness of "cross sets," height, then dune heights (α|) ranged from 32 – 56 (reported in ms as 30 – 60 cm).

Water depth was estimated using the formulation of Bridge and Tye (2000): $d = 11.6h_m^{0.84}$ where d is water depth, and h_m is mean dune height (32 – 56 cm)

Slope was estimated using "Method 1" of Lynds et al. (2014): $S = 1.65D_{50}/H_{bf}$, where S is slope; D_{50} is the mean 50th percentile of the bed load samples, and H_{bf} is the bankfull water depth. D_{50} = 0.24 mm; H_{bf} = 5 m.

Paleocurrent Data

Small scale X-stratification

Locality	ID	Adjusted for Declination SS	Plunge	Corrected data - azimuth	Corrected, rotated data - azimuth	Corrected data - plunge
N30.06202-W115.78037	53	165	0	164.1	155.5	-9.4

[1]Supplemental Material. Consists of petrographic data, calculations of sedimentological parameters (bedform height; water depth; slope), and paleocurrent data. Please visit https://doi.org/10.1130/GEOS.S.12331337 to access the supplemental material, and contact editing@geosociety.org with any questions.

clayskins (cutans), suggesting illuviation in a B-horizon setting (Fig. 12C). Here, as in Facies 2, the dominant clay species is illite.

Most distinctive in Facies 3—but not necessarily characterizing all of it—are carbonate nodules. These range in diameter from several cm to ~1 mm. They are generally aligned vertically in a weakly linear way, with some coarsest sizes associated with the upper contacts of bedding, and successively smaller sizes descending (Fig. 12D). They commonly preserve a central core, likely to have been the root around which they developed. They are distinct from carbonate concretions, also preserved in the FTS, which tend to be larger, less spherical, are horizontally oriented (commonly, in association with textural discontinuities between beds), and lack the vertical trending quality clearly visible in the descending associations of nodules. With calcite evidently mobilized diagenetically as cements (see above), these concretions are interpreted here as postdepositional, and thus unconnected with the active pedogenesis in this paleoenvironment.

Facies 3 exhibits evidence of significant bioturbation in some localities, such that all primary sedimentary features have been obliterated (Fig. 13A). The burrows are not large, generally between 2 and 5 mm in diameter, and traceable as far as 6 cm. Trace fossil burrows are common; they are not uniformly vertically oriented; many contain at least a portion that is subhorizontal. These burrows are superficially similar to those produced by insects in alluvial environments (Hasiotis and Bown, 1992); however, truly diagnostic features are lacking. Larger, vertically oriented conically shaped burrows are preserved as well; some of these are as much as 20 cm long (deep) and 6 cm in diameter (Fig. 13B). These, however, are preserved exclusively in Facies 1, and compare favorably burrows of the crayfish ichnogenus *Camborygina* sp. (Hasiotis and Mitchell, 1993).

Interpretation. Facies 3 is a carbonate nodule-bearing paleosol facies. The color banding is best interpreted as the remnants of pedogenic subsurface horizons, where the mottling (Fig. 12B) is associated with a fluctuating water table, producing changing Eh and pH conditions that ultimately control the stability of dissolved ferric oxyhydroxides

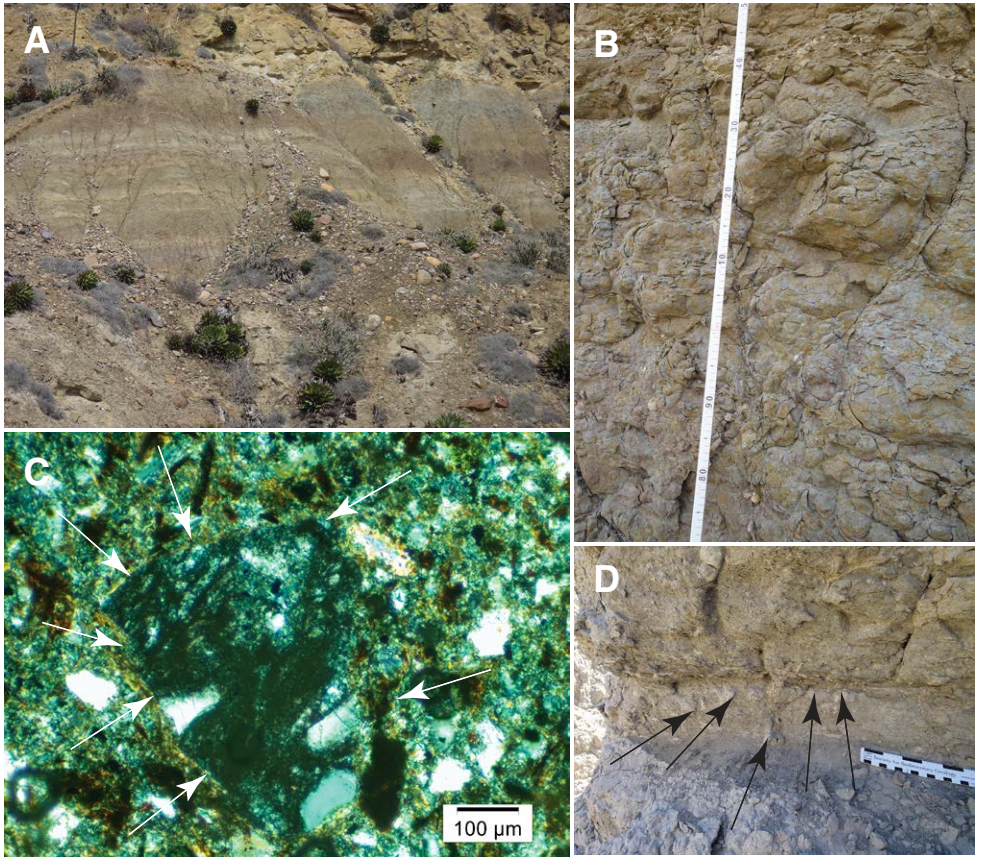

Figure 12. Facies 3, Paleosols. (A) Paleosol horizons in outcrop identified by color banding; (B) mottling in inferred compound B-horizon sequence, exemplifying compound pedogenesis in these paleosols; (C) photomicrograph showing cutans forming around a sedimentary lithic clast (highlighted by arrows); (D) densely packed, partially coalesced carbonate nodules (arrows) associated with a rooted horizon. Upper part of scale in inches; lower in cm. Fossiliferous terrestrial sequence (FTS), El Disecado Member, El Gallo Formation, Baja California, México.

(Buol et al., 1980). Using the classification from the Soil Survey Staff (1975), the mottles would be classified as "many," of medium size, and "distinct" in contrast; however, FTS diagenesis has clearly modified these features from their original condition in the active soil.

The presence of carbonate (calcite) nodules accords with a fluctuating water table perhaps due to limited rainfall; in the vertically oriented suites of nodules, translocated solubilized carbonates were likely associated with the movement of materials through the soil in and out of the roots, but during drier times, rainfall would have been insufficient to solubilize and remove the carbonate ions, which then would precipitate and accumulate as calcite (see Retallack, 2001).

A distinctive feature of the FTS paleosols is that they preserve the clear imprint of compound pedogenesis (e.g., Duchafour, 1991) such that superficial horizons, such as O and A horizons,

are almost never recognizable. In most cases, all definitive traces of them have been removed, either through erosion, oxidization, or through re-purposing as subsurface horizons. What remains are thick (multi-meter) sequences of rooted, ped-bearing, mottled Bt horizons. Ultimately, compound pedogenesis and the absence of preserved diagnostic criteria hinder classification of these paleosols (Mora et al., 1993). Here, therefore, the features that we observe allow us to recognize some key processes these soils, which in turn allow us to infer aspects of the paleoenvironments in which they formed (see Retallack, 2001):

(1) Extensive mottling suggests the presence of fluctuating moisture (and, likely, Eh and pH) conditions in the soil subsurface.
(2) Peds, horizonation, cutans, and carbonate nodules, dominate the paleosols; these suggest active soil processes (in particular, illuviation) occurring in well-developed soils.
(3) Therefore, by contrast to Facies 1 and 2, Facies 3 represents zones of relative landscape stability in an otherwise episodically depositional setting.

Other Sedimentary Features

Although Faces 1 and 3 dominate the sedimentation of the FTS, several other sedimentary features are noteworthy as well. Plant material is found in several settings. In La Amarilla, large pieces of silicified wood, syndepositionally unpetrified, were carried as clasts within the active channels (Fig. 8D; see description of Facies 1 above). Unsilicified plant material is also present in fine-grained settings preserving small, floodplain ponds, identifiable by distinctive organic-rich (dark-colored), fine-grained, thin-bedded (<0.5 m), laminated silty mudstones associated with paleosol deposits. In such settings, delicate roots, leaves, and stems are preserved (Fig. 5A at the 12.03 mark; Fig. 14); we interpret these to be highly localized, low-energy floodplain ephemeral(?) pond deposits.

Pollen is abundant throughout the FTS. It is commonly preserved in darker, finer-grained deposits such as those associated with Facies 3;

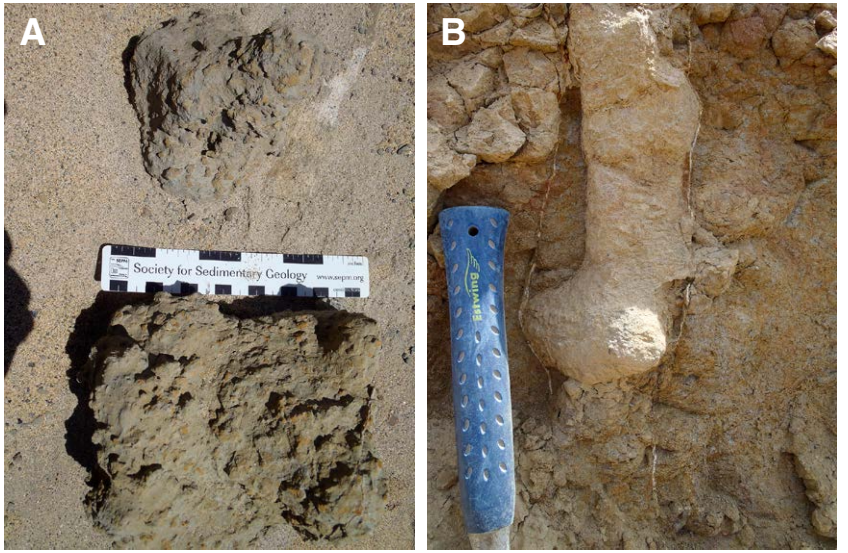

Figure 13. Terrestrial trace fossil bioturbation, fossiliferous terrestrial sequence (FTS), El Disecado Member, El Gallo Formation, Baja California, México. (A) Small traces referable to colonial arthropods such as termites (Hasiotis and Bown, 1992). (B) Large burrows referable to the crayfish ichnogenus *Camborygina* sp. (Hasiotis and Mitchell, 1993). Smaller traces tend to be oriented variably in space; larger trace fossils uniformly oriented vertically. In A, upper part of scale in inches; lower in cm. In B, blue handle is 19 cm in length.

Figure 14. Plant root fragments from laminated claystones, interpreted to represent deposition in a highly localized floodplain pond.

however, it is not generally a component of Facies 2. A diverse palynomorph assemblage is preserved in the FTS; however, describing it is beyond the scope of this study.

Finally, several plant localities exist, dominated largely by ferric oxyhydroxide-replaced angiosperm fruits (O. Cornales: *Operculifructus*; Hayes et al., 2018). Some of these localities consist of lenticular deposits of fine-grained laminated silt or fine sandstones postdepositionally ferric oxyhydroxide-cemented; others are clearly developed in Facies 3 (paleosols) as indicated by iron mottling of the siltstones. Iron-replaced roots, carbonate nodules, and iron-cemented horizons are commonly associated with these localities. The presence of well-developed soil features associated with these concentrations of plant material suggests that at these localities, at least, the plant materials are autochthonous.

Basal Lithology—"Ambar"

Description. As noted above, the most basal exposures in this study here begin in, and just landward of the Pacific Ocean. These consist of a sequence we dubbed "Ambar," which lies conformably beneath the FTS. Ambar is composed of interbedded cross-stratified sandstones and mudstones, with extensive burrowing (Fig. 15). These are tubular in shape, ~1 cm in diameter, and up to 15 cm in depth. Backfilling spreite are clearly visible. The backfilled burrows are relatively densely packed, with each burrow separated by a few cm. These burrows are comparable to *Skolithos*, a well-known Phanerozoic marginal-marine trace fossil morphotype attributed to vermiform animals such as polychaetes (see Dodd and Stanton, 1990; Desjardins et al., 2010; Herringshaw et al., 2010; Vinn and Wilson, 2013). Other types of burrows are also present; these are narrower and include a horizontal component as well as a vertical one.

Interpretation. "Ambar" bears a suite of facies—largely, bioturbated, organic-rich sandstones and mudstones—suggesting biotic activity, but it does not present any of the three major facies described above, nor does it contain any of the indicators

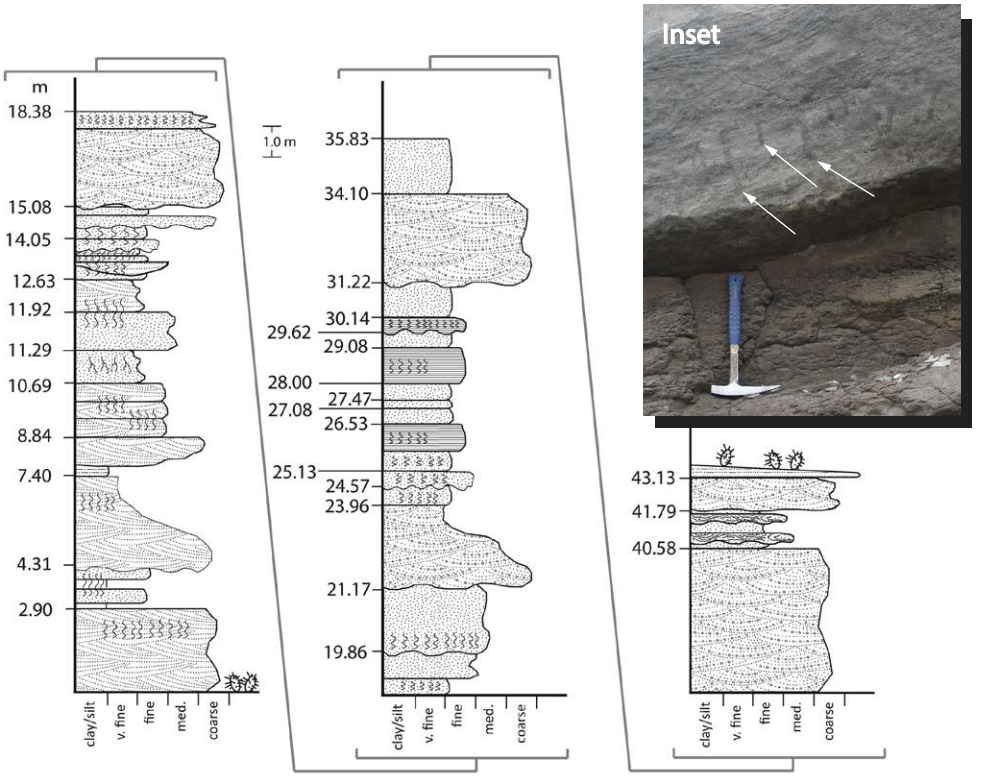

Figure 15. The "Ambar" locality (DEF060614-1), interpreted here as a marginal marine setting (see text). Symbols as in Figure 5. The base of the fossiliferous terrestrial sequence (FTS) can be reliably placed at 31.22 m. Inset: *Skolithos* trace fossils (three marked with arrows).

of terrestriality (e.g., paleosols and terrestrial vertebrate fossils; see below). It does, however, contain palynomorphs, charcoal, and some small amber deposits, indicating proximity to terrestrial environments.

Limited outcrop exposure constrains the certitude with which the sedimentary environments represented at this locality can be identified here; however, an interpretation that is concordant with the features it presents is that of a marginal marine setting, such as a tidal flat. Among the observations in agreement with this interpretation are (a) thick sequences of fine-grained, organic-rich mudstones; (b) the extensive burrowing of a limited number (only two types) of trace fossil, reflective of high-abundance, low-diversity paleoecology characteristic of similar stressed environments; (c) channelized fine-grained sandstones, which in this setting would represent tidal channels; (d) extensive bioturbation, of typically marginal marine aspect (Rhoads, 1975).

Vertebrate Assemblages

The immediate impetus for understanding the paleoenvironmental setting of these deposits was the vertebrate fossil faunas that have been recovered from them. The most productive facies are La Amarilla and GF. La Amarilla produces relatively

TABLE 2. DISTRIBUTION OF MICROVERTEBRATES RECOVERED FROM FTS (SEE FIG. 15)

Taxon	Counts	%
Vertebrata *indet*.	501	31
Dinosauria	250	16
Theropoda	97	6
Saurischia	10	0.6
Ornithischia	178	11
Reptilia *indet*.	43	3
Testudines	249	16
Squamata	114	7
Crocodylia	127	8
Amphibia	22	1
Non-Tetrapoda	1	0.06
Mammalia	8	0.5
Total	1600	100

large dinosaur bones; most commonly, disarticulated limb bones and isolated vertebrae of adult hadrosaurs, although other substantial bones, such as a variety of turtle, have been found. Collections of large vertebrates were also made during the 1960s by paleontologists from the Los Angeles County Museum (Morris, 1973, 1981). Vertebrates notwithstanding, the most common fossil in La Amarilla is petrified wood. We did not collect La Amarilla systematically for fossil content, and thus our observations here about La Amarilla are anecdotal.

The most productive facies for microvertebrates is GF. To date, 87 fossil localities have been recorded in the FTS (Fig. 1). Since 2004, GF has each year been systematically screen washed. The microvertebrates GF produces are generally very small (1–2 mm; taxonomically identifiable fragments are less common, but average ~15 mm), disarticulated, and commonly fragmentary. There are rare exceptions to this, including the semi-articulated remains of the squamate *Dicothodon* (Montellano-Ballesteros et al., 2005; Chavarría-Arellano et al., 2018a, 2018b), the tooth-bearing jaws of several vertebrates, and a near-complete multituberculate (mammal) skull (Wilson et al., 2011). However, although GF cannot be said to be rich in microvertebrates, after 14 years of collecting (as of this writing), a substantial microvertebrate assemblage has emerged, comprising some 1600 individual specimens (see Table 2; Fig. 16). This includes rays, at least two families of teleosts, amphibians including frogs and salamanders (Romo de Vivar Martínez et al., 2016), at least five different taxa of turtles (López-Conde et al., 2018) including the characteristic *Naomichelys speciosa*, plus *Basilemys* sp., *Compsemys victa*, Trionychidae indet., and cf. Chelydridae, at least four families of lizards (Chavarría-Arellano et al., 2018a, 2018b), crocodylomorphs, several families of theropod and ornithischian dinosaurs, and multituberculate and eutherian mammals (Romo de Vivar Martínez, 2011; García-Alcántara, 2016).

Finally, the FTS contains a few potentially in situ vertebrate fossils along with the preponderance of allochthonous specimens. Several interesting, and semi-articulated fossil specimens—notably a partial and fragmented baby hadrosaur and eggshell fragments—have been found at contacts between GF and the paleosol facies (Cabrera-Hernández, 2018; Cabrera-Hernández et al., 2018). These fossils breathe promise of nesting in the ancient FTS distal fan, a possibility that requires further exploration.

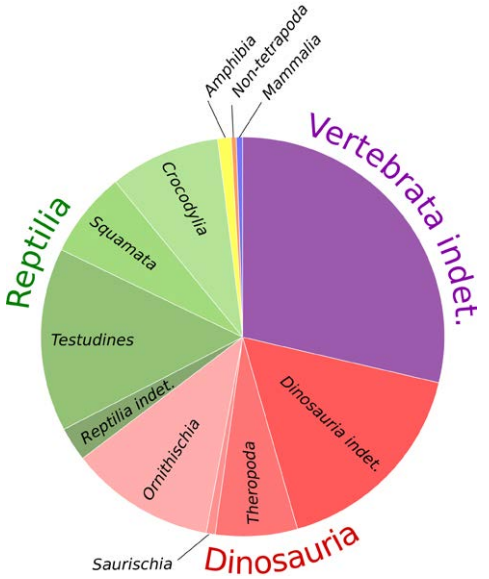

Figure 16. Distribution of microvertebrates, fossiliferous terrestrial sequence (FTS), El Disecado Member, El Gallo Formation, Baja California, México. Table 2 gives percentages of key groups.

Stable Isotopes

Carbon- and oxygen-isotope data for hadrosaurid tooth enamel and dentine and from paleosol carbonate nodules from the FTS are reported in Table 3.

Two methods demonstrate that our results are primary: (1) an isotopic comparison of dentine and enamel from the same element; (2) an isotopic comparison of enamel carbonate and authigenic carbonate (i.e., paleosol nodules).

These comparisons rest on the assumption that the isotopic characteristics of dentine and paleosol nodules represent the burial and/or diagenetic environment, and if the isotopic characteristics of tooth materials are different, then the tooth enamel is

TABLE 3. ISOTOPIC DATA FROM HADROSAUR TOOTH ENAMEL, DENTINE, AND PALEOSOL CARBONATE NODULES (SEE FIG. 18)

Hadrosaur tooth enamel			Hadrosaur tooth dentine			Paleosol nodule micrite		
Sample	$\delta^{13}C$	$\delta^{18}O$	Sample	$\delta^{13}C$	$\delta^{18}O$	Sample	$\delta^{13}C$	$\delta^{18}O$
EGF H1E	–8.4	25.2	EGF H1D	–7.4	24.5	EGF-1-N1	–10.4	20.7
EGF H2E	–9.9	24.9	EGF H1D	–10.6	23.5	EGF-1-N2	–9.5	19.7
EGF H3E	–10.7	25.5	EGF H7D	–4.1	24.7	EGF-2-N1	–10.9	21.6
EGF H4E	–8.5	26.4	EGF H8D	–4.9	24.0	EGF-2-N1	–6.4	18.1
EGF H5E	–8.9	24.8				EGF-2-N1	–11.2	21.5
EGF H6E	–9.6	24.7				EGF-2-N1	–11.6	21.0
						EGF-2-N1	–10.2	21.2
						EGF-2-N1	–11.1	21.6

likely preserving primary biological information. Dentine is more susceptible to diagenesis when compared to tooth enamel because of its higher porosity and larger apatite surface area; pedogenic nodules are by definition authigenic. A clear difference in both $\delta^{13}C$ and $\delta^{18}O$ between tooth enamel and paleosol carbonate (Table 2), as well as a difference in $\delta^{13}C$ between tooth enamel and tooth dentine (Table 2), permit the conclusion that primary isotopic information is preserved in tooth enamel carbonate.

With confidence, then, that our isotopic results are primary, we integrated the FTS results with those previously published from the more northern and eastern sites, which allowed us to investigate latitudinal patterns in stable isotopic ratios. Figure 18 shows that there is a negative correlation between latitude and $\delta^{18}O$ and a positive correlation between latitude and $\delta^{13}C$ for both tooth enamel and nodules, with the highest $\delta^{18}O$ and lowest $\delta^{13}C$ being associated with the Baja locality. $\delta^{13}C$ values from co-occurring tooth enamel and nodules broadly overlap at every locality where they are found together. Similar overlap is also observed in $\delta^{18}O$ for the Two Medicine and Kaiparowits Formations, but not in the FTS, where $\delta^{18}O$ of nodules is significantly lower than that of tooth enamel.

DISCUSSION

Environment of Deposition

The FTS represents a fully terrestrial setting. Supporting this are (1) the presence of a diverse terrestrial vertebrate and plant assemblage with no evidence of marine influence (see below); (2) the presence of well-developed paleosols, which in life were unambiguously subaerial features of the landscape; and (3) the presence of a suite of sedimentary features commonly associated with fluvial environments.

Both Facies 1 and 2 are the products of high-energy, unstable landscapes. However, as we have seen, considerable evidence for landscape stability exists in the form of the well-developed sequences of paleosols forming with compound pedogenesis (Facies 3). Time of formation of soils is notoriously difficult to estimate; however, the presence of well-developed sequences of peds, horizons, cutans, and root-originated carbonate nodules suggests significant time intervals of landscape stability. We interpret Facies 3 as floodplain deposition, representing land surfaces that likely functioned on multi-century timescales.

Ancient Flow Directions in the FTS

Some of the paleocurrent data (Fig. 10) show a direction opposite to the dominant trends in the data (e.g., south- and east-directed). We interpret this as the presence of tidal influence in this setting. Directionally bimodal cross-stratification is most commonly associated with tidal successions (e.g., Boggs, 2001); here, however, we propose that strong tidal bores likely made their way up some of the channels, producing sigmoidal cross stratification with slipface mud-couplets, features associated with tidal deposits (Prothero and Schwab, 2004) and recorded in La Amarilla (Fig. 17). The existence of tidal bores in the braided channels may have contributed to the unusually broad range of paleocurrent trends recorded and reinforces the interpretation of the FTS as a marginal marine deposit.

Paleocurrent data collected for this study show a strong pattern of northward flow, with a modest westward component. Unsurprisingly, sedimentary structures representing the largest bedforms show the least variation. These data imply, however, that at least the proximal source for the FTS was to the south, but results do not precisely accord with those obtained from Fulford and Busby's (1993) limited (n = 11) data set for this member, in which a NW trend was obtained, or with their larger-scale results for the entire El Gallo Formation, in which they recognized a broad (nearly 180°) spread of paleocurrents (from a much larger database; n = 264), with a west-directed mean and considerable circular dispersion. They interpreted their results as concordant with a broad braid plain draining into a Cretaceous proto–Pacific Ocean.

Several possible scenarios could explain the more northern (and less western) trends of the paleocurrents we obtained. Scenario 1 is that the FTS was not in its present orientation, and that it has rotated as much as 90° from its Cretaceous position. Nothing in the known regional deformation would suggest that this occurred. In Scenario 2, the fossiliferous outcrops studied here may reflect local geography, and whereas overall

Figure 17. Signoidal cross stratification with well-developed fine-sand couplets, fossiliferous terrestrial sequence (FTS), El Disecado Member, El Gallo Formation, Baja California, México.

depositional trends were likely westward, here, a local, small-scale northward depositional feature is being recorded.

Geomorphic Setting: Distal Subaerial Fan?

Petrographically as well as geographically, the active arc magmatic setting of the FTS suggests that it represents the geomorphic and depositional interface between the magmatic arc and the proto–Pacific Ocean. Because this likely involved the emergence of a channel draining mountains in combination with evidence for episodic and sheet flooding (Bull, 1972), a subaerial fan setting is suggested. The sandstones of the FTS are petrographically and compositionally immature, suggesting relative proximity to the source, and the fine-grained and sedimentary aspect of the system is also potentially concordant with the relatively distal component of a subaerial fan system.

While Miall (2006) regards fans as geomorphically unique rather than embodying unique sedimentary facies, Blair and McPherson (1994) note that in process, bedforms, sedimentary deposits as well as geomorphology, fans differ dramatically from other kinds of terrestrial/fluvial deposits. Their work details a broad list of fan features, including piedmont setting, the emergence of piedmont channels to unconfined flow, transport along the fan by mass-wasting and fluvial processes, rare and episodic deposition, the presence of poorly sorted, angular gravels, steep flow gradients, a "plano-convex" cross section (perpendicular to fan growth), a decrease in slope with distance from the source, and an absence of well-developed floodplains. These features, they aver, make fans unique among terrestrial depositional environments, and they reject what they perceive as a tendency of certain sedimentologists to merge braided river deposits with alluvial fans.

Indeed, the FTS contains retrievable features not associated by Blair and McPherson (1994) with fan deposition, most notably the absence of gravels, the presence of fine-grained sedimentation organized in well-developed floodplain deposits, and extremely low slopes. These features, however, are in agreement with the outer-fan setting of the "Low Sinuosity/Meandering Fluvial Fan" model of Stanistreet and McCarthy (1993). In this model, distal depositional slopes are predicted to be low (~0.0003), comparable to that reported here for the FTS (0.00008). The disarticulated microvertebrate fauna, almost exclusively confined to the sheet-flow deposits, and macrovertebrate faunal elements (largely, but not exclusively hadrosaur bones), carried in the Facies 1 channels along with large tree trunks, reinforce the suggestion of episodic, high-energy flooding in a relatively stabilized coastal floodplain setting.

In summary, distinctive features that unambiguously characterize fans primarily rooted in geomorphology and process (Blair and McPherson, 1994) are either unretrievable in the FTS deposits, or are distinctly muted in this inferred distal setting, although episodicity and unconfined (sheet flood) deposition are preserved. Thus while acknowledging that the fit of the FTS to ideal arid fan deposits (Blair and McPherson, 1994) is imperfect, we tentatively propose a distal fan environment, such as that suggested by Stanistreet and McCarthy (1993) as a potential paleoenvironmental setting for the FTS. A marginal marine relationship is suggested by the stratigraphic proximity of marginal marine deposits to the FTS sedimentary package.

Climate

Carbonate nodules and soil-matrix mottling seen in paleosol Bt horizons send a clear signal of wet/dry cyclicity in the soil subsurface; cyclicity that most likely derived from the climate in which these soils developed. We infer generally dry conditions from the stable isotopic results (see below); however, as noted above, there is evidence for laterally restricted ponding on the floodplains (above; see Figs. 5A [at the 12.03 mark] and 14).

Vertebrate Taphonomy

The fragmentary, disarticulated quality of the vertebrates, and their marked correspondence to facies—large fossils in La Amarilla and microvertebrates within GF—strongly suggests that these fossils were carried into this system as allochthonous clasts in approximate hydraulic equivalence with flow. In La Amarilla, fossils—both vertebrate and plant—are organized in clear relationship to the cross-stratification and are associated with the scour fills that form at the toes of migrating three-dimensional subaqueous dunes. In GF, the fossils approximately match the size of the largest clasts in the system, and like them are chaotically distributed within it. They therefore must represent an upper limit of the competence of these debris flows; however, because they are potentially less dense than the other clasts in GF, we cannot determine whether they are associated with the larger clasts in matrix support, or whether they are themselves part of the matrix, otherwise composed of smaller, denser clasts.

Although the vertebrate fossils are certainly not in situ (they are clasts carried in the sedimentary system), their relatively fresh (not water-worn) condition suggests minimal travel; that is, they may have lived in association on the distal fan environment described here; however, smaller clasts (including allochthonous fossils), generally, show less rounding than larger clasts in siliciclastic depositional systems. Microvertebrate remains, including parts of a semi-articulated postcranial elements and a semi-articulated skull of two perinatal hadrosaurs (Fig. 5A;Cabrera-Hernández, 2018 and Cabrera-Hernández et al., 2018), are known from paleosol (Facies 3) deposits in the FTS, suggesting that, by contrast, facies GF most likely concentrated the fossils, rather than carried them from a long distance away. If this is true, their disarticulated quality potentially results from surficial gathering of isolated bones on the fan braid plains during storm events.

Stable Isotopes

Fricke et al. (2008, 2009) compared stable isotopic data from North American, late Campanian, terrestrial, dinosaur-bearing formations, including the Two Medicine, Judith River, Dinosaur Park,

Kaiparowits, and Fruitland Formations with the goal of studying dinosaur migration; from these, they reconstructed a latitudinal gradient in isotope ratios. Given the late Campanian age of the FTS, as well as the fact that oceanic carbon isotope ratios varied by only ~0.25‰ and temperature varied by only ~1–2 °C during the late Campanian (Barrera and Savin, 1999), integrating FTS data into those from the Western Interior of the United States is a natural and logical step.

Spatial Patterns in $\delta^{13}C$ and $\delta^{18}O$

The lack of isotopic overlap between samples from the FTS and other Campanian localities (Table 3; Fig. 18) is consistent with the FTS hadrosaurids being ecologically distinct from the other records reported in Fricke et al. (2009, 2015), an expected result given the location of the FTS on the Pacific side of the Cordillera. These differences stem from the $\delta^{13}C$ of vegetation they were eating and $\delta^{18}O$ of water they were drinking.

$\delta^{13}C$. One of the most remarkable aspects of the carbon isotope data presented in Table 3 and Figure 18 is the wide range in $\delta^{13}C$ values of hadrosaur tooth enamel, and by extension, the wide range in $\delta^{13}C$ values of Late Cretaceous vegetation. Assuming a $\delta^{13}C$ offset between diet and tooth enamel of 19‰ for hadrosaurs (Fricke, 2007), average values for vegetation range from ~22‰ in coastal settings in Montana and Alberta to ~25‰ in more upland environments of Montana and Utah, to ~29‰ in Baja. Taken together, this range in values is similar to that observed for modern C3 plants (e.g., O'Leary et al., 1992) and suggests that both now and in the past, the same factors operated to produce a range in $\delta^{13}C$ values of modern C3 plants. Such factors include: (1) environmental variables that influence water availability to a plant, such as rainfall, humidity, salinity, and location in the canopy (e.g., sun versus shade); (2) the $\delta^{13}C$ of the atmosphere, and (3) taxon-specific differences in fractionation during the process of photosynthesis (e.g., O'Leary et al., 1992).

Environmental variables such as the amount of precipitation are generally considered to play a dominant role in influencing plant $\delta^{13}C$, and several relations have been developed between precipitation and $\delta^{13}C$, with higher $\delta^{13}C$ corresponding to drier conditions (e.g., Diefendorf et al., 2010). Such relations would suggest that El Gallo landscapes were wetter than those farther north; however, this interpretation is inconsistent with sedimentological data. The Judith River, Dinosaur Park, and Fruitland Formations contain coal and lignite beds, whereas the Kaiparowits and Two Medicine Formations include lake deposits; by contrast, the FTS shows evidence of wet/dry cyclicity and significant drainage in its paleosols. All of these observations suggest that the more northern localities were wetter than the El Gallo.

It is possible, therefore, that the $\delta^{13}C$ of the atmosphere under some forest canopies differed from that of the open atmosphere due to inputs of soil-respired CO_2. This canopy effect is associated with dense, closed canopies, and has been observed to produce leaves with unusually low $\delta^{13}C$ (e.g., van der Merwe and Medina, 1991). For this factor to play a dominant role in explaining the spatial patterns in Figure 18, FTS forests would have to have had the most recycling of soil-respired CO_2, and thus be the densest. Again, it is hard to reconcile this interpretation with the sedimentological evidence, which suggests that FTS landscapes were dominated by braided fluvial systems that were prone to episodic sedimentation associated with high flow intensities. In addition, organic matter is less common in the FTS than in its northern and eastern counterparts, suggesting a lack of vegetation that contrasts with the organic-rich deposits to the north.

A third, and perhaps the most likely, explanation for the wide range in $\delta^{13}C$ is that different plant types dominated different landscapes. In particular, it is observed today that angiosperm plants typically have $\delta^{13}C$ values that are 1‰–2‰ lower than that of gymnosperm plants (e.g., Heaton, 1999), thus a larger proportion of angiosperms to gymnosperms in Baja relative to other localities could explain the lower $\delta^{13}C$ values observed there (Fig. 18). It is tantalizing, but hardly conclusive, that—aside from indeterminate petrified wood—the most common plants preserved in the FTS are angiosperm fruits (Hayes et al., 2018). Moreover, because angiosperms are thought to have evolved and undergone extensive radiation from low- to high latitudes during the mid- to Late Cretaceous (Wing and Boucher, 1998), and it has been posited

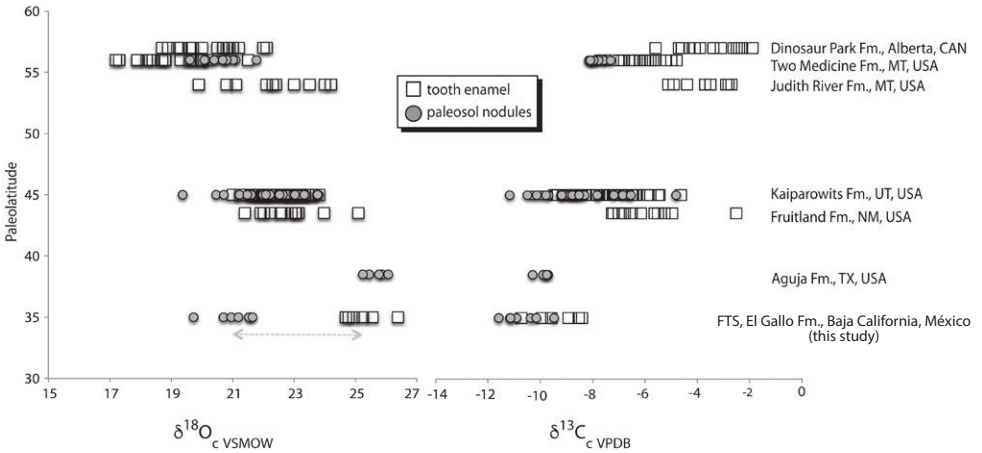

Figure 18. Comparison of carbonate isotope data from seven different Campanian-aged fossil-bearing formations and localities in western North America (see Table 3). Note that the fossiliferous terrestrial sequence (FTS) fauna was located to the west of the Cordillera, while the other localities were to the east of it.

that they were able to do so because of their ability to occupy disturbed habitats (Wing and Boucher, 1998). FTS habitats may have been populated by a greater proportion of angiosperm taxa than were their counterparts to the north and east. FTS landscapes, located to the south of the others and dominated by avulsing river systems and episodic debris flows, could have been occupied by a flora assemblage much different than those localities to the north.

δ¹⁸O. Considering all the hadrosaur $\delta^{18}O$ data together, a gradual decrease in $\delta^{18}O$ with latitude is observed (Fig. 18). Such patterns in $\delta^{18}O$ of precipitation are observed today, and at global scales are attributed to the gradual rainout of moisture from airmasses as they move from low to high latitudes (e.g., Rozanski et al., 1993). Precipitation patterns over western North America during the Campanian were, however, complicated by the existence of the Sevier highlands and of the Western Interior Seaway (e.g., Sewall and Fricke, 2013). Therefore regional-scale patterns in atmospheric movement and rainout may also account for some of the difference in $\delta^{18}O$ observed in Figure 18. Indeed, Baja California del Sur was located on the western, windward side of the Cordillera, whereas all other sites were located leeward of the highlands and on the coast of the Western Interior Seaway. As a result, Baja California was dominated by Pacific-sourced airmasses that would have experienced little rainout prior to landfall such that $\delta^{18}O$ of precipitation remained high, whereas localities to the north and east were more likely to have precipitation sourced from both Pacific and Western Interior Sea–sourced air masses (Sewall and Fricke, 2013). In reaching the eastern side of the Cordillera, Pacific-sourced air masses would have undergone extensive distillation, thus producing much lower $\delta^{18}O$ in Alberta and Montana.

What is more unusual about the $\delta^{18}O$ data is the large offset in $\delta^{18}O$ between paleosol carbonate nodule and hadrosaur tooth enamel, not observed at the other northern and eastern localities. Although the $\delta^{18}O$ of tooth enamel from a homeothermic hadrosaur is presumably insensitive to temperature, the $\delta^{18}O$ of authigenic soil nodules is not. Thus, one possible explanation of a larger difference in $\delta^{18}O$ is that nodules formed at higher temperatures in FTS soils relative to other localities with nodules. Because nodules today are observed to form at the onset of the dry season when evaporation-induced precipitation of calcite takes place (e.g., Breecker et al., 2009), the implication is that dry seasons in Baja were significantly warmer than those at other locations. Perhaps these warmer temperatures are indicative of a more seasonally extreme climate in the region, an inference which is concordant with its observed sedimentological characteristics (e.g., episodic sedimentation, and wet/dry cyclicity) relative to the other late Campanian localities studied.

CONCLUSIONS

The FTS, ~130 m of terrestrial, fossil-bearing sedimentation in the upper part of the El Disecado Member of the El Gallo Formation, Baja California, México, is an important, heretofore unknown southern and western locality producing faunas and floras of late Campanian age in North America. The FTS represents a fully terrestrial environment, tentatively, a marginal-marine distal arid fan characterized by high-energy, episodic sedimentation. It likely developed in association with the then-nascent Peninsular Range of central and northern Baja California, and prograded out against the proto–Pacific Ocean of the late Campanian, an inference we derive from the close stratigraphic proximity of a marine unit ("Ambar") conformably at its base. The FTS is stratigraphically dissected by cross-stratified, well-sorted channelized medium sand-sized sand bodies, suggesting high flow intensities and low-sinuosity fluvial channels.

Petrographically, FTS sediments are characterized by compositional and textural immaturity, reflecting relative proximity to the source. In the scheme of Dickinson and Suczek (1979), clast compositions indicate a magmatic arc, an inference that is concordant with the paleogeographic setting. Grain sizes are uniformly fine, suggesting some geographic separation from the source. A strong sedimentary lithic component pervades all samples, reinforcing the idea of some transport and associated reworking.

Along with the high-energy, episodic deposition, well-developed, thick, sequences of compound paleosols preserving subsurface horizons contain evidence of a fluctuating water table, implying a climatic regime that was characterized by wet/dry cyclicity, and likely tied to the episodicity of the sedimentation. Actively flowing water deposited FTS sedimentary rocks; however, the presence of extensive carbonate nodule development in the subsurface horizons suggests that episodes of aridity characterized this environment.

Deposition direction inferred from the dip orientations of the cross stratification reveals some circular dispersion, but was generally to the north; somewhat unexpected in this coastal setting, in which broadly west-directed flow might be anticipated. A local peculiarity of geomorphologic setting, however, could be responsible for the strong northern component of the deposition. We also found significant small-scale eastward flow, likely reflecting tidal influence.

The taphonomy and sedimentology of the FTS suggest that most of the individuals there were not preserved in situ, in that the faunas are generally disarticulated, and their bones found under conditions in which they would not likely have lived (active flowing fluvial channels and sheet-flow debris deposits associated with storm events). Two distinct size classes of vertebrate fossils are preserved: large vertebrate elements (e.g., hadrosaur femora; isolated vertebrae, etc.) and microvertebrate remains, generally 1–3 mm in size but, among diagnosable fossils, averaging ~15 mm. The large fossil elements are associated with fluvial channel deposits, whereas the microvertebrates are strikingly correlated with fine-grained sheet-flow deposits. Floras in the FTS are relatively common, and at several localities, small (~1 cm in diameter) multi-seed, spherical infructescences referred to the angiosperm genus *Operculifructus* (O. Cornales) are commonly preserved (Hayes et al., 2018). These are found tightly associated with other plant remains in paleosol deposits, suggesting that they, in contrast to the vertebrates, may be autochthonous in origin. Rare plant macrofossils, other than the ubiquitous, allochthonous silicified woody trunks found in the braided channel deposits, are

preserved in laminated, lenticular clay-rich, mudstone deposits, suggesting preservation in local floodplain ponds.

Analyses of stable isotopic ratios of hadrosaur teeth and primary calcitic nodules demonstrate that isotopic paleolatitude trends established in other late Campanian localities farther to the north and west extend into the FTS, the most westerly and southward locality of the suite. Although a number of factors might account for the paleolatitude-correlated shifts, the simplest and most likely explanation is that the floras eaten by the hadrosaurs varied latitudinally, and this is reflected in both their isotopic content, and that of the dinosaurs that ate them. That the FTS, at least, contains a floral assemblage different from that of its coeval northern and eastern counterparts is hinted by the presence of *Operculifructus* infructescences preserved there (Hayes et al., 2018), a cornalean genus unknown from the localities well to the north and east of Baja California in which originally the latitudinal stable isotopic trends were originally identified (Fricke et al., 2009).

ACKNOWLEDGMENTS

We gratefully acknowledge generous support by the Programa de Apoyo a Proyectos de Investigación e InnovaciónTecnológica, for IN 100913 "Fauna de microvertebrados de la formación El Gallo (Cretácico Tardío, Campaniano) Baja California, México" and IN103616 "Microvertebrados de la formación El Gallo y algunos aspectos paleoambientales con base en isótopos estables de C y O" to Dr. Montellano, as well as by the Departamento de Paleontología, Instituto de Geología, Universidad Nacional Autónoma de México. We also acknowledge generous support of Franklin Research grants from the American Philosophical Society and a University of Washington College of Arts and Sciences grant to G. Wilson. Special thanks are owed to Dra. T. Pi, Instituto de Geología, Universidad Nacional Autónoma de México, for her detailed analysis of the clays in Facies 2 (GF), and to Dr. Simon Engelhart, University of Durham, UK, for his help with the grain-size analysis. We thank the faculty who participated in the field work along the way: Jesús Alvarado, Enrique Martínez, and Jeffrey A. Wilson. We also thank all the students who participated in the field seasons and helped collect the fossil material (K. Ángeles-Ortíz, D.J. Cabrera-Hernández, M.L. Chavarría-Arellano, M. Chen, M. de Sosa, D. García-Alcántara, A. García-Gil, M.T. González-Cruz, O. López-Conde, M.L. Martín-Aguilar, J. Barrientos, and V. Zavaleta-Villarreal), as well as the many students who picked fossils from matrix in the Instituto de Geología paleontological laboratory. We particularly wish to acknowledge the contributions of *las familias* Rojas and Acevedo, without whose support in El Rosario, this work could not have been carried out. University of Rhode Island (URI) undergraduate C. Tiley carried out the analyses in Figure 15 and Table 1 and constructed the figure. The stable isotopic laboratory work in the United States was supported, in part, by the Department of Geosciences, URI, and by the Geological Society of America. U-Pb geochronology was supported through National Science Foundation grant EAR-1424892 to JR (Sam Bowring). Special thanks are due to J.P. Battacharya for his thoughtful, careful review; this work benefitted greatly from his efforts.

REFERENCES CITED

Barrera, E., and Savin, S.M., 1999, Evolution of late Campanian-Maastrichtian marine climates and oceans, *in* Barrera, E., and Johnson, C.C., eds., Evolution of the Cretaceous Ocean–Climate System: Geological Society of America Special Paper 332, p 242–282, https://doi.org/10.1130/0-8137-2332-9.245.

Bhattacharya, J.P., Copeland, P., Lawton, T., and Holbrook, J., 2016, Estimation of source area, river paleo-discharge, paleoslope, and sediment budgets of linked deep-time depositional systems and implications for hydrocarbon potential, *in* Walsh, J.P., Wiberg, P., and Aalto, R., eds., Source-to-Sink Systems: Sediment and Solute Transfer on the Earth Surface: Earth-Science Reviews, v. 153, p. 77–110, https://doi.org/10.1016/j.earscirev.2015.10.013.

Blair, T.C., and McPherson, J.G., 1994, Alluvial fans and their natural distinction from rivers based on morphology, hydraulic processes, sedimentary processes, and facies assemblages: Journal of Sedimentary Research, v. 64, p. 450–489.

Boggs, S., 2001, Principles of Sedimentary Geology (3rd ed.): New Jersey, Prentice Hall, 726 p.

Boothroyd, J.C., and Ashley, G.M., 1975, Processes, bar morphology, and sedimentary structures on braided outwash fans, northeastern Gulf of Alaska, *in* Jopling, A.V., and McDonald, B.C., eds., Glaciofluvial and Glaciolacustrine Sedimentation: SEPM Special Publication no. 23, p. 193–222, https://doi.org/10.2110/pec.75.23.0193.

Bowring, J.F., McLean, N.M., and Bowring, S.A., 2011, Engineering cyber infrastructure for U-Pb geochronology: Tripoli and U-Pb_Redux: Geochemistry, Geophysics, Geosystems, v. 12, QOAA19, https://doi.org/10.1029/2010GC003479.

Breecker, D.O., Sharo, Z.D., and McFadden, L.D., 2009, Seasonal bias in the formation and stable isotopic composition of pedogenic carbonate in modern soil from central New Mexico, USA: Geological Society of America Bulletin, v. 121, p. 630–640, https://doi.org/10.1130/B26413.1.

Bridge, J.S., 2003, Rivers and Floodplains: Forms, Processes, and Sedimentary Record: Malden, Massachusetts, Blackwell Publishing, 491 p.

Bridge, J.S., and Tye, R.S., 2000, Interpreting the dimensions of ancient fluvial channel bars, channels, and channel belts from wireline-logs and cores: The American Association of Petroleum Geologists Bulletin, v. 84, p. 1205–1228.

Bull, W.B., 1972, Recognition of alluvial-fan deposits in the stratigraphic record, *in* Rigby, J.K., and Hamblin, W.K., eds., Recognition of Ancient Sedimentary Environments: Society of Economic Paleontologists and Mineralogists Special Publication no. 16, p. 63–83, https://doi.org/10.2110/pec.72.02.0063.

Buol, S.W., Hole, F.D., and McCracken, R.J., 1980, Soil Genesis and Classification: Ames, Iowa, Iowa State University Press, 406 p.

Busby, C.J., 2004, Continental growth at convergent margins facing large ocean basins: A case study from Mesozoic convergent-margin basins of Baja California, Mexico: Tectonophysics, v. 392, p. 241–277, https://doi.org/10.1016/j.tecto.2004.04.017.

Busby, C.J., Smith, D.P., Morris, W.R., and Adams, B., 1998, Evolutionary model for convergent margins facing large ocean basins: Mesozoic Baja California (Mexico): Geology, v. 26, p. 227–230, https://doi.org/10.1130/0091-7613(1998)026<0227:EMFCMF>2.3.CO;2.

Busby, C.J., Yip, G., Blikra, L., and Renne, P., 2002, Coastal landsliding and catastrophic sedimentation triggered by Cretaceous–Tertiary bolide impact: A Pacific margin example?: Geology, v. 30, p. 687–690, https://doi.org/10.1130/0091-7613(2002)030<0687:CLACST>2.0.CO;2.

Cabrera-Hernández, J., 2018, Descripción e identificación de cáscaras de huevo de dinosaurios fósiles y de dos dinosaurios perinatales de la formación El Gallo (Cretácico tardío) El Rosario, Baja California, México [B.S. thesis]: Jalisco, México, Universidad de Guadalajara. Centro Universitario de Ciencias Biológicas y Agropecuarias. Zapopan, 113 p.

Cabrera-Hernández, J.S., Hernández-Rivera, R., and Montellano-Ballesteros, M., 2018, Fossil eggshells and two perinatal dinosaurs from the El Gallo Formation (Late Cretaceous), El Rosario, Baja California, Mexico: Journal of Vertebrate Paleontology, v. 38, no. 3, p. 100.

Chavarría-Arellano, M.L., García-Alcántara, D., Romo de Vivar, P., and Montellano-Ballesteros, M., 2018a, Lizards from El Gallo formation (Campanian), Baja California, Mexico: Journal of Vertebrate Paleontology, v. 38, no. 3, Supplement, p. 104.

Chavarría-Arellano, M.L., Simões, T.R., and Montellano-Ballesteros, M., 2018b, New data on the Late Cretaceous lizard *Dicothodon bajaensis*: Annals of the Brazilian Academy of Sciences, v. 90, no. 3, https://doi.org/10.1590/0001-3765201820170563.

Collinson, J.D., 1996, Alluvial sediments, *in* Reading, H.G., ed., Sedimentary Environments: Processes, Facies, and Stratigraphy: Malden, MA, Blackwell Publishing, p. 37–82.

Condon, D.J., Schoene, B., McLean, N.M., Bowring, S.A., and Parrish, R.R., 2015, Metrology and traceability of U-Pb isotope dilution geochronology (EARTHTIME Tracer Calibration Part I): Geochimica et Cosmochimica Acta, v. 164, p. 464–480, https://doi.org/10.1016/j.gca.2015.05.026.

DeMets, C., and Merkouriev, S., 2016, High-resolution reconstructions of Pacific-North America plate motion: 20 Ma to present: Geophysical Journal International, v. 207, p. 741–773, https://doi.org/10.1093/gji/ggw305.

Desjardins, P.R., Mángano, M.G., Buatois, L.A., and Pratt, B.R., 2010, *Skolithos*: Lethaia, v. 43, p. 507–528, https://doi.org/10.1111/j.1502-3931.2009.00214.x.

Dickinson, W.R., and Suczek, C.A., 1979, Plate tectonics and sandstone compositions: The American Association of Petroleum Geologists Bulletin, v. 63, p. 2164–2182.

Diefendorf, A.F., Mueller, K.E., Wing, S.L., Koch, P.L., and Freeman, K.H., 2010, Global patterns in leaf ^{13}C discrimination and implications for studies of past and future climate: Proceedings of the National Academy of Sciences of the United States of America, v. 107, p. 5738–5743, https://doi.org/10.1073/pnas.0910513107.

Dodd, J.R., and Stanton, R.J., Jr., 1990, Paleoecology: Concepts and Applications (2nd ed.): New York, John Wiley and Sons, 502 p.

Duchafour, P., 1991, Pedology: soil, vegetation, and environment: Masson, Paris, 448 p.

Fraser, G.S., and Suttner, L., 1986, Alluvial fans and fan deltas: Boston, International Human Resources Development Corporation, 199 p.

Fricke, H., Montellano, M., Wilson, G.P., Sewall, J.O., Sertich, J., and Fastovsky, D.E., 2015, Looking over the Late Cretaceous Cordillera: A comparison of stable isotope records and climate model simulations from Utah and New Mexico with those from Baja California, Mexico: Geological Society of America Abstracts with Programs, v. 47, no. 7, p. 172.

Fricke, H.C., 2007, Stable isotope geochemistry of bonebed fossils: Reconstructing paleoenvironments, paleoecology, and paleobiology, *in* Rogers, R.R., Eberth, D.A., and Fiorillo, A.R., eds., Bonebeds: Genesis, Analysis, and Paleobiological Significance: Chicago, Illinois, University of Chicago Press, p. 437–490, https://doi.org/10.7208/chicago/9780226723730.003.0008.

Fricke, H.C., Rogers, R.R., Backlund, R., Dwyer, C.N., and Echt, S., 2008, Preservation of primary stable isotope signals in dinosaur remains, and environmental gradients of the Late Cretaceous of Montana and Alberta: Palaeogeography, Palaeoclimatology, Palaeoecology, v. 266, p. 13–27, https://doi.org/10.1016/j.palaeo.2008.03.030.

Fricke, H.C., Rogers, R.R., and Gates, T.A., 2009, Hadrosaurid migration: Inferences based on stable isotope comparisons among Late Cretaceous dinosaur localities: Paleobiology, v. 35, no. 2, p. 270–288, https://doi.org/10.1666/08025.1.

Fulford, M.M., and Busby, C.J., 1993, Tectonic controls on non-marine sedimentation in a Cretaceous fore-arc basin, Baja California, Mexico, *in* Frostick, L.E., and Steel, R.J., eds., Tectonic Controls and Signatures in Sedimentary Successions: Special Publication no. 20, International Association of Sedimentologists: Boston, Blackwell Scientific Publications, p. 301–333.

García-Alcántara, D., 2016, Microvertebrados de Fiesta de Huesos, El Rosario, Baja California [B.S. thesis]: Universidad Nacional Autónoma de México, Facultad de Ciencias, México.

Graham, J., 1988, Collection and analysis of field data, *in* Tucker, M., ed., Techniques in Sedimentology: Boston, Blackwell Scientific Publications, p. 5–62.

Hajek, E.A., and Heller, P.L., 2012, Flow-depth scaling in alluvial architecture and nonmarine sequence stratigraphy: example from the Castlegate Sandstone, central Utah, USA: Journal of Sedimentary Research, v. 82, p. 121–130, https://doi.org/10.2110/jsr.2012.8.

Harms, J.C., Southard, J.B., and Walker, R.G., 1982, Structures and Sequences in Clastic Rocks: Tulsa, Oklahoma, SEPM (Society for Sedimentary Geology), Short Course no. 9, 249 p., https://doi.org/10.2110/scn.82.09.

Hasiotis, S.T., and Bown, T.M., 1992, Invertebrate trace fossils: the backbone of continental ichnology, *in* Maples, C.G., and West, R.R., eds., Trace Fossils: Short Courses in Paleontology Number 5, Paleontological Society, p. 64–104.

Hasiotis, S.T., and Mitchell, C.E., 1993, A comparison of crayfish burrow morphologies: Triassic and Holocene fossil, paleo- and neo-ichnological evidence, and the identification of their burrowing signatures: Ichnos, v. 2, p. 291–314, https://doi.org/10.1080/10420949309380104.

Hayes, R., Smith, S.Y., Montellano-Ballesteros, M., Álvarez-Reyes, G., Hernandez-Rivera, R., and Fastovsky, D.E., 2018, Cornalean affinities, phylogenetic significance, and biogeographic implications of *Operculifructus*: American Journal of Botany, v. 105, p. 1911–1928, https://doi.org/10.1002/ajb2.1179.

Heaton, T.H.E., 1999, Spatial, species, and temporal variations in the $^{13}C/^{12}C$ ratios of C_3 plants: Implications for paleodiet studies: Journal of Archaeological Science, v. 26, p. 637–649, https://doi.org/10.1006/jasc.1998.0381.

Herringshaw, L.G., Sherwood, O.A., and McIlory, D., 2010, Ecosystem engineering by bioturbating polychaetes in event bed microcosms: Palaios, v. 25, p. 46–58, https://doi.org/10.2110/palo.2009.p09-055r.

Hiess, J., Condon, D.J., McLean, N., and Noble, S.R., 2012, $^{238}U/^{235}U$ Systematics in Terrestrial Uranium-Bearing Minerals: Science, v. 335, no. 6076, p. 1610–1614, https://doi.org/10.1126/science.1215507.

Jaffey, A.H., Flynn, K.F., Glendenin, L.E., Bentley, W.C., and Essling, A.M., 1971, Precision Measurement of Half-Lives and Specific Activities of ^{235}U and ^{238}U: Physical Review. C, v. 4, no. 5, p. 1889–1906, https://doi.org/10.1103/PhysRevC.4.1889.

Kilmer, F.H., 1963, Cretaceous and Cenozoic Stratigraphy and Paleontology, El Rosario Area, Baja California, Mexico [Ph.D. thesis]: University of California, Berkeley, 216 p.

Krogh, T.E., 1973, Low-Contamination Method for Hydrothermal Decomposition of Zircon and Extraction of U and Pb for Isotopic Age Determinations: Geochimica et Cosmochimica Acta, v. 37, no. 3, p. 485–494, https://doi.org/10.1016/0016-7037(73)90213-5.

Kuiper, K.F., Deino, A., Hilgen, F.J., Krijgsman, W., Renne, P.R., and Wijbrans, J.R., 2008, Synchronizing rock clocks of Earth history: Science, v. 320, p. 500–504, https://doi.org/10.1126/science.1154339.

Leclair, S.F., and Bridge, J.S., 2001, Quantitative interpretation of sedimentary structures formed by river dunes: Journal of Sedimentary Research, v. 71, p. 713–716, https://doi.org/10.1306/2DC40962-0E47-11D7-8643000102C1865D.

López-Conde, O., Brinkman, D., Sterli, J., Chavarría-Arellano, M.L., and Montellano-Ballesteros, M., 2018, Turtles from the Late Cretaceous (Campanian) of El Gallo Formation, Baja California, Mexico: Journal of South American Earth Sciences, v. 88, p. 693–699, https://doi.org/10.1016/j.jsames.2018.10.005.

Lowe, D.R., 1979, Sediment gravity flows: their classification and some problems of application to natural flows and deposits, *in* Doyle, L.J., and Pilkey, O.H., eds., Geology of Continental Slopes: SEPM Special Publication no. 27, p. 75–82, https://doi.org/10.2110/pec.79.27.0075.

Lynds, R.M., Mohrig, D., Hajek, E.J., and Heller, P.L., 2014, Paleoslope reconstruction in sandy suspended-load-dominant rivers: Journal of Sedimentary Research, v. 84, p. 825–836, https://doi.org/10.2110/jsr.2014.60.

Mattinson, J.M., 2005, Zircon U/Pb chemical abrasion (CATIMS) method: Combined annealing and multi-step partial dissolution analysis for improved precision and accuracy of zircon ages: Chemical Geology, v. 220, no. 1–2, p. 47–66, https://doi.org/10.1016/j.chemgeo.2005.03.011.

McLean, N.M., Bowring, J.F., and Bowring, S.A., 2011, An algorithm for U-Pb isotope dilution data reduction and uncertainty propagation: Geochemistry, Geophysics, Geosystems, v. 12, https://doi.org/10.1029/2010GC003478.

McLean, N.M., Condon, D.J., Schoene, B., and Bowring, S.A., 2015, Evaluating uncertainties in the calibration of isotopic reference materials and multi-element isotopic tracers (EARTHTIME Tracer Calibration Part II): Geochimica et Cosmochimica Acta, v. 164, p. 481–501, https://doi.org/10.1016/j.gca.2015.02.040.

Miall, A.D., 1977, A review of the braided river depositional environment: Earth-Science Reviews, v. 13, p. 1–62, https://doi.org/10.1016/0012-8252(77)90055-1.

Miall, A.D., 1978, Lithofacies types ad vertical profile models in braided river deposits: A summary, *in* Miall, A.D., ed., Fluvial Sedimentology: Canadian Society of Petroleum Geologists Memoir no. 5, p. 1613–1632.

Miall, A.D., 2006, The Geology of Fluvial Deposits: New York, Springer, 582 p., https://doi.org/10.1007/978-3-662-03237-4.

Min, K., Mundil, R., Renne, P.R., and Ludwig, K.R., 2000, A test for systematic errors in $^{40}Ar/^{39}Ar$ geochronology through comparison with U/Pb analysis of a 1.1-Ga rhyolite: Geochimica et Cosmochimica Acta, v. 64, no. 1, p. 73–98, https://doi.org/10.1016/S0016-7037(99)00204-5.

Mohrig, D., Heller, P.L., Paola, C., and Lyons, W.J., 2000, Interpreting avulsion process from ancient alluvial sequences: Guadalope-Matarranya system (northern Spain) and Wasatch Formation (western Colorado): Geological Society of America Bulletin, v. 112, p. 1787–1803, https://doi.org/10.1130/0016-7606(2000)112<1787:IAPFAA>2.0.CO;2.

Montellano-Ballesteros, M., Wilson, G., Hernandez-Rivera, R., Quintero, E., and Aranda-Manteca, F., 2005, New material of *Polyglyphanodon bajaensis*: Journal of Vertebrate Paleontology, v. 25, p. 93A.

Mora, C.I., Fastovsky, D.E., and Driese, S.G., 1993, Geochemistry and stable isotopes of paleosols (Short Course Manual): University of Tennessee Department of Geological Sciences Studies in Geology, no. 23, 66 p.

Morris, W.J., 1973, Mesozoic and Tertiary vertebrates in Baja California: National Geographic: Research Reports (Montgomery), v. 1966, p. 197–209.

Morris, W.J., 1981, A new species of hadrosaurian dinosaur from the upper Cretaceous of Baja California: ?*Lambeosaurus laticaudus*: Journal of Paleontology, v. 55, p. 453–462.

Munsell Soil Color Charts, 1992, Macbeth Division of Kollmorgen Instruments Corp., Newburgh, New York.

O'Leary, M.H., Mahavan, S., and Paneth, P., 1992, Physical and chemical basis of carbon isotope fractionation in plants: Plant, Cell & Environment, v. 15, p. 1099–1104, https://doi.org/10.1111/j.1365-3040.1992.tb01660.x.

Pierson, T.C., and Costa, J.E., 1987, A rheological classification of subaerial sediment-water flows, *in* Costa, J.E., and Wieczorek, G.F., eds., Debris Flows/Avalanches: Process, Recognition, and Mitigation: Geological Society of America Reviews in Engineering Geology, v. VII, p. 1–12.

Prothero, D.R., and Schwab, F., 2004, Sedimentary Geology: New York, W.H. Freeman & Company, 557 p.

Ramezani, J., Hoke, G.D., Fastovsky, D.E., Bowring, S.A., Therrien, F., Dworkin, S.I., Atchley, S.C., and Nordt, L.C., 2011, High-precision U-Pb zircon geochronology of the Late Triassic Chinle Formation, Petrified Forest National Park (Arizona, USA):

Temporal constraints on the early evolution of dinosaurs: Geological Society of America Bulletin, v. 123, p. 2142–2159, https://doi.org/10.1130/B30433.1.

Renne, P.R., Fulford, M.M., and Busby-Spera, C., 1991, High resolution $^{40}Ar/^{39}Ar$ chronostratigraphy of the Late Cretaceous El Gallo Formation, Baja California del Norte, Mexico: Geophysical Research Letters, v. 18, p. 459–462, https://doi.org/10.1029/91GL00464.

Retallack, G.J., 2001, Soils of the Past: An Introduction to Paleopedology: Malden, Massachusetts, Blackwell Science, 404 p., https://doi.org/10.1002/9780470698716.

Rhoads, D.C., 1975, The paleoecological and environmental significance of trace fossils, *in* Frey, R.W., ed., The Study of Trace Fossils: New York, Springer-Verlag, p. 147–160, https://doi.org/10.1007/978-3-642-65923-2_9.

Romo de Vivar Martínez, P.R., 2011, Microvertebrados cretácicos tardíos del área de El Rosario, Baja California, México [B.S. thesis]: Universidad Nacional Autónoma de México, Facultad de Ciencias.

Romo de Vivar Martínez, P.R., Montellano Ballesteros, M., and García Alcántara, D., 2016, Primer registro de la Familia Albanerpetontidae (Lissamphibia) en la formación El Gallo (Campaniano), Baja California, México: Boletín de la Sociedad Geológica Mexicana, v. 68, p. 571–580, https://doi.org/10.18268/BSGM2016v68n3a11.

Rozanski, K., Araguás-Arguás, L., and Gonfiantini, R., 1993, Isotopic patterns in modern global precipitation, *in* Swart, P.K., Lohmann, K.C., McKenzie, J., and Savin, S., eds., Climate Change in Isotopic Records: Geophysical Monograph, v. 78, https://doi.org/10.1029/GM078p0001.

Rubin, D.M., and McCulloch, D.S., 1980, Single and superimposed bedforms: A synthesis of San Francisco Bay and flume observations: Sedimentary Geology, v. 26, p. 207–231, https://doi.org/10.1016/0037-0738(80)90012-3.

Sewall, J., and Fricke, H.C., 2013, Andean-scale highlands in the Late Cretaceous Cordillera of the North American western margin: Earth and Planetary Science Letters, v. 362, p. 88–98, https://doi.org/10.1016/j.epsl.2012.12.002.

Soil Survey Staff, 1975, Soil Taxonomy: Washington, D.C., U.S. Department of Agriculture Handbook no. 436, U.S. Government Printing Office.

Stanistreet, I.G., and McCarthy, T.S., 1993, The Okavango fan and the classification of subaerial fan systems: Sedimentary Geology, v. 85, p. 115–133, https://doi.org/10.1016/0037-0738(93)90078-J.

Thomas, R.G., Smith, D.G., Wood, J.M., Visser, J., Calverley-Range, E.A., and Koster, E.H., 1987, Inclined heterolithic stratification—Terminology, description, interpretation and significance: Sedimentary Geology, v. 53, p. 123–179.

van der Merwe, N.J., and Medina, E., 1991, The canopy effect, carbon isotope ratios and foodwebs in Amazonia: Journal of Archaeological Science, v. 18, p. 249–259, https://doi.org/10.1016/0305-4403(91)90064-V.

Vinn, O.V., and Wilson, M.A., 2013, An event bed with abundant *Skolithos* burrows from the late Pridoli (Silurian) of Saaremaa (Estonia): Carnets de Géologie, Lettre CG2013_L02, p. 83–87.

Wilson, G., Meng, C., and Montellano-Ballesteros, M., 2011, A new multituberculate skull from the Upper Campanian "El Gallo Formation," Baja California, Mexico. IV Congreso Latinoamericano de Paleontología de Vertebrados, San Juan, Argentina, September, 2011: Ameghiniana, v. 48, no. 4, Supplement, p. R115.

Wing, S.L., and Boucher, L.D., 1998, Ecological aspects of the Cretaceous flowering plant radiation: Annual Review of Earth and Planetary Sciences, v. 26, p. 379–421, https://doi.org/10.1146/annurev.earth.26.1.379.